Quantitative trait locus mapping of osmotic stress response in the fungal wheat pathogen *Zymoseptoria tritici*

Authors:

Jessica Stapley and Bruce A. McDonald

Plant Pathology Group, Institute of Integrative Biology, ETH Zurich, 8092 Zürich, Switzerland

Corresponding author: Jessica Stapley, Jessica.stapley@usys.ethz.ch

Abstract

Osmotic stress is a ubiquitous and potent stress for all living organisms, but few studies have investigated the genetic basis of salt tolerance in filamentous fungi. The main aim of this study was to identify regions of the genome associated with tolerance to potassium chloride in the wheat pathogen *Zymoseptoria tritici.* A secondary aim was to identify candidate genes affecting salt tolerance within the most promising chromosomal regions. We achieved these aims with a quantitative trait locus (QTL) mapping study using offspring from two crosses grown in vitro in the presence or absence of osmotic stress imposed by 0.75M KCl. We identified significant QTL for most of the traits in both crosses. Several QTL overlapped with QTL identified in earlier studies for other traits and some QTL explained trait variation in both the control and salt stress environments. A significant QTL on chromosome 3 explained variation in colony radius at 8 days post inoculation (dpi) in the KCl environment as well as colony radius KCl tolerance at 8 dpi. The QTL peak had a high LOD and encompassed an interval containing only 36 genes. Six of these genes present promising candidates for functional analyses. A GO enrichment analysis of QTL unique to the KCl environment found evidence for enrichment of functions involved in osmotic stress responses.

Keywords:
Salt stress; plant pathogen; fungi; *Mycosphaerella graminicola*, QTL

34 **Introduction**

35 Osmotic stress is a common and potent environmental stress that can limit growth and
36 reproduction in many organisms. At the cellular level osmotic stress results in changes to
37 the movement of water into or out of the cell through osmosis. To counteract osmotic
38 stress, organisms need to accumulate compatible solutes (e.g. glycerol, erythritol, arabitol,
39 mannitol and trehalose) – that can balance osmosis and provide turgor pressure (Kogej *et al.*
40 2007; Araújo *et al.* 2020). In fungal pathogens of plants, the pathogen may be exposed to a
41 relatively high salt concentration (0.5M) within the plant (see Araújo et al., 2020) as well as
42 experience changes in salt and osmolyte concentrations as plant tissues degrade (Jacob *et*
43 *al.* 2015). The genes and pathways involved in responding to the resulting osmotic stresses
44 may also affect plant-pathogen interactions and virulence. For example, turgor pressure
45 which is mediated by changes in vacuole size and number is important in both plant tissue
46 penetration and response to osmotic stress (Richards *et al.* 2010). Genes involved in cell
47 wall integrity and remodelling, e.g. glycoside hydrolases, can mediate osmotic stress
48 response and virulence (Li *et al.* 2016). Voltage-gated chloride channels, which are involved
49 in the regulation of cell volume, also influence virulence in fungal pathogens of both plants
50 and humans (Zhu and Williamson 2003; Cañero and Roncero 2008). Knowledge of the
51 genetic basis of osmotic sensitivity in plant pathogens can thus provide insights into the
52 genetic basis of environmental stress responses as well as disease development.
53
54 The immediate effects of osmotic stress in fungi include stalled growth, changes in the
55 recruitment of water, collapse of the cytoskeleton, altered plasma membranes and a
56 reduction in glycerol transport (Hohmann 2002; Duran *et al.* 2010). Longer-term adaptation
57 to osmotic stress involves modifications of metabolism, plasma membranes, cell wall
58 thickness and cell wall melanisation, as well as an accumulation of mycosporines (Hohmann
59 2002; Kogej *et al.* 2007). Osmotic stress is also likely to activate many genes and pathways
60 involved in the 'general stress response'. For example, up to 10% of the genes that were
61 differentially expressed under different individual stressors were shared across different
62 osmotic stress treatments (Hohmann 2002). Stress response regulators and genes such as
63 HSP90 and GTPase *Ras1* are considered promising antifungal drug targets for human
64 pathogens (LeBlanc *et al.* 2020). These proteins may also become fungicide targets for plant

65 pathogens as our understanding of the molecular mechanisms governing stress responses in
66 plant pathogenic fungi improves.
67
68 Although the key salt stress response pathways and genes have been identified and well
69 characterized in model yeasts, studies in filamentous fungi could provide novel insights into
70 the genes involved in responding to osmotic stress. The HOG pathway is an osmoresponsive
71 system and one of the most well-understood mitogen-activated protein (MAP) kinase
72 pathways (Hohmann 2002). In yeast, two genes are central components of this pathway –
73 Pbs2 and Hog1p kinase. In plant pathogens, HOG signalling appears more complex than in
74 yeast, although it is still poorly understood (Jacob *et al.* 2015). Several filamentous
75 pathogenic fungi, including our model *Zymoseptoria tritici*, have multiple (up to 17) histidine
76 kinases, whereas *S. cerevisiae* has only one (Sln1p) (Jacob *et al.* 2015). Several studies have
77 identified transcription factors (TFs) involved in regulating the fungal response to salt stress,
78 as well as other stressors - including temperature and fungicide stress. For example, in
79 *Aspergillus oryzae*, GATA TFs were shown to be important in responding to salt and
80 temperature stress (Jiang *et al.* 2021). In the causal agent of Fusarium head blight (*Fusarium*
81 *graminearum*), the nutrient and stress factor 1 (NSf1) C_2H_2 zinc fingers protein plays an
82 important role in salt stress response, sexual-asexual reproduction, vegetative growth,
83 fungicide sensitivity and pathogenicity (Shi *et al.* 2021), and a Zn(2)-C6 fungal-type DNA-
84 binding TF (Fss1) is required for sodium and lithium tolerance (Son *et al.* 2015). Cell wall
85 melanisation also appears to confer benefits for osmotic stress tolerance. For example, cell
86 wall melanisation in halotolerant fungi helps to maintain high concentrations of glycerol and
87 contain the resulting turgor pressure by strengthening and preventing leakage through the
88 cell wall (Kogej *et al.* 2007). These examples coming from a relatively small number of fungal
89 species demonstrate how the molecular mechanisms of salt response can vary across taxa
90 and illustrate that additional work is needed to understand how filamentous fungi adapt to
91 salt stress.
92
93 To improve our understanding of osmotic stress response in fungi we performed a
94 quantitative trait loci (QTL) mapping study using the wheat pathogen *Z. tritici* growing under
95 salt stress. QTL studies have been instrumental in finding candidate genes for multiple traits
96 in this widespread and damaging wheat pathogen, including melanisation (Lendenmann *et*

97 *al.* 2014), fungicide sensitivity (Lendenmann *et al.* 2015), morphological switching (Francisco
98 *et al.* 2023) and oxidative stress (Zhong *et al.* 2021), and enabled the cloning and functional
99 validation of genes affecting virulence (Zhong et al., 2017; Meile et al. 2018), melanisation
100 (Krishnan et al. 2018), and morphological switching (Francisco *et al.* 2023). QTL mapping
101 identifies genomic regions that explain variation in a trait and that are likely to harbour
102 genes responsible for creating variation in the trait. The aim of this study was to identify
103 large effect loci associated with tolerance to salt stress in *Z. tritici* and identify plausible
104 candidate genes within the most promising QTL intervals.
105
106 **Methods**
107 **QTL mapping crosses**
108 Parent and progeny isolates used in this study are from two crosses that were described
109 previously (Lendenmann *et al.* 2014). The original choice of strains for making crosses was
110 based upon a comprehensive phenotyping campaign of an international collection of 150
111 strains, including 30 strains from Switzerland (Zhan *et al.* 2005). In this original phenotyping
112 campaign, we measured seven traits for each strain, including in planta virulence and
113 pycnidia size and density, and growth rates in vitro under different temperatures and in the
114 presence of fungicides. Based on data from these seven traits, four Swiss strains were
115 selected to make the QTL mapping crosses that yielded 700 offspring over the two crosses.
116 The four parents have since been tested under other environmental stressors (e.g. reactive
117 oxygen (Zhong *et al.* 2021)) including KCl (0.25-1.0M). In the presence of 0.75M KCl the
118 parents differed in both growth and melanisation traits (unpublished data). The crosses
119 were made by coinfecting wheat leaves with the parent strains, with the resulting
120 ascospores collected from infected leaves and grown in vitro. One cross was between
121 ST99CH1A5 and ST99CH1E4 (herein referred to as 1A5 and 1E4 respectively) and the other
122 was between ST99CH3D7 and ST99CH3D1 (herein referred to as 3D7 and 3D1 respectively).
123
124 **Genotyping**
125 SNP genotype data for the progeny were obtained from a RAD sequence dataset that was
126 previously produced in our lab (first described in (Lendenmann *et al.* 2014). In brief, the
127 genome was cut using the restriction enzyme *Pst*I and the libraries were sequenced on an
128 Illumina HiSeq2000 with paired-end sequencing. Complete genome sequences of the

129 parental strains (Croll *et al.* 2013)(NCBI Biosample: SRS383146 (ST99CH3D1), SRS383147
130 (ST99CH3D7), SRS383142 (ST99CH1A5), and SRS383143 (ST99CH1E4)) were used to SNP
131 genotype the parents and offspring.
132
133 RADseq processing and variant discovery is described in detail at
134 https://github.com/jessstapley/QTL-mapping-Z.-tritici. In brief, RADseq reads were trimmed
135 of adaptors and low-quality sequence using trimmomatic (v0.35). The RADseq reads were
136 mapped to a reference genome using bwa mem (v0.7.17). Reads from progeny of the
137 3D7x3D1 cross were mapped to the 3D7 reference genome and progeny from the 1A5x1E4
138 cross were mapped to the 1A5 reference genome. Variant calling was done using the GATK
139 Germline Short Variant Discovery pipeline, following their Best Practice recommendations
140 (https://gatk.broadinstitute.org/hc/en-us/sections/360007226651-Best-Practices-
141 Workflows). After this we applied the following filters: only biallelic SNPs, parents had
142 alternative alleles, <50% missing genotypes per marker, <50% missing genotypes per
143 individual, mean read depth >3 and <30, depth quality (QD)>5, mapping quality >40, minor
144 allele frequency >0.02 and <0.80, and SNPs in regions where the SNP density is >3 in 10bp
145 were removed.
146
147 **Generating linkage maps**
148 Linkage maps were made using R (R Core Team 2020), R Studio (RStudio Team 2020) and
149 the R package qtl (v1.48-1 (Broman *et al.* 2003)). As the order and base pair positions of the
150 markers were known from the reference genomes, we only needed to calculate the
151 recombination distance between markers to create the linkage map. Before map
152 construction, we removed putative clones. To do this we calculated genetic similarity using
153 the 'comparegeno' function and removed individuals with >99% shared genotypes (83
154 progeny were removed from the 1A5x1E4 cross, 74 progeny were removed from the
155 3D7x3D1 cross). The linkage map was constructed for each chromosome separately using
156 the 'estimatemap' function with method 'morgan'. Then we performed multiple rounds of
157 cleaning to remove error-prone markers that caused map inflation. First, we removed
158 markers that had an estimated recombination distance above the 99.9% quantile. Then
159 recombination rate was estimated again and we inspected the maps. In regions of the map
160 where there was evidence of map inflation and spurious double recombination events, we

161 visualised these regions in an Integrated Genome Viewer (IGV, https://igv.org) to look at the
162 mapping alignments. Markers were removed from regions with poor alignments and
163 evidence of mismapping. A summary of the two linkage maps is provided in Supplementary
164 Table S1 and the complete maps are available at (https://github.com/jessstapley/QTL-
165 mapping-Z.-tritici). After applying all of these filters, the average marker spacing was 1217
166 bp (0.19 cM) and 529 bp (0.14 cM) for the 1A5x1E4 and 3D7x3D1 crosses, respectively.
167
168 **Phenotyping**
169 We compared colony growth and melanisation in a control environment and in the
170 presence of potassium chloride (KCl) to simulate a salt stress environment. Potassium
171 chloride (KCl) has been used extensively in the study of stress responses in fungi because it
172 is environmentally ubiquitous and lacks the toxic effects of Na^+ (Hohmann 2002; Araújo *et*
173 *al.* 2020). Only non-clonal offspring strains were phenotyped (for 1A5x1E4 n= 259 strains;
174 for 3D7x3D1 n=265 strains). The basic protocols for isolate recovery from -80^{0}C storage,
175 growth in vitro and the measurements of colony size and colony melanisation were
176 described previously (Zhong *et al.* 2021). In brief, Petri dishes containing Difco potato
177 dextrose agar (PDA) were inoculated with 200µl of a spore solution (concentration 200
178 spores/ml) and grown at 18^{0}C for 8 and 12 days. In the salt stress environment, a sterile
179 potassium chloride solution was added to the cooled and sterilized PDA to make a final
180 concentration of 0.75M. Three replicates were grown in both the control and salt (KCl)
181 environments.
182
183 Two traits were measured; colony area and colony grey value, using automated image
184 analysis as described previously (Lendenmann *et al.* 2014; Zhong *et al.* 2021). Grey value
185 was measured on a scale of 0-255, where darker, more melanised colonies have lower
186 values (0 = black, 255 = white). Mean colony area (mm^2) and grey value were calculated
187 from measurements of multiple colonies on each plate and then the mean was calculated
188 across the three replicate plates to obtain a final mean colony area and mean grey value for
189 each strain in the two environments. Colony area was converted to colony radius by dividing
190 by π and taking the square root of this value. Measurements were taken at 8- and 12-days
191 post inoculation (dpi). For the analysis we used three different types of data; (1) time
192 point/age: the colony radius and grey value at 8 and 12 dpi; (2) daily rate measurements:

193 the change in colony radius or grey value between 8 and 12 dpi (i.e. the difference in colony
194 radius between 8 and 12 dpi/difference in days); and (3) KCl tolerance measurements: the
195 ratio of a measurement (colony radius, grey value, growth rate or melanisation rate)
196 between the KCl environment and the control environment (i.e. colony radius KCl tolerance
197 at 8 dpi = colony radius at 8 dpi in the KCl environment/colony radius at 8 dpi in the control
198 environment, or growth rate KCl tolerance = growth rate in the KCl environment/growth
199 rate in the control environment). For the KCl tolerance measurements, values >1 indicate
200 that for that trait an isolate is more tolerant to KCl (higher value under salt stress), and
201 values <1 indicate that for that trait measured an isolate is more sensitive to KCl. In total
202 there were 18 traits (Table 1).
203
204 **QTL mapping and analysis of genes within QTL intervals**
205 QTL mapping was performed using the R (v 3.6.0) package 'qtl2' (v2_0.24) as described in
206 detail on github (https://github.com/jessstapley/QTL-mapping-Z.-tritici). We scanned the
207 genome for a single QTL per chromosome with the '*scan1*' function using a linear mixed
208 effect model, and we controlled for the relatedness of individuals (i.e. we included a
209 random polygenic effect) by fitting the kinship matrix as a random effect. Models that take
210 into account the genetic covariance between individuals can reduce the false discovery rate
211 in QTL scans and outperform models that do not include this information in the model
212 (Malosetti *et al.* 2011). The significance threshold for a QTL peak was determined by
213 permutation tests (n=1000) and we calculated a Bayes Credible Interval (95%) to identify the
214 interval size around the QTL peak. We used custom R scripts to extract a list of the genes
215 within the interval from the annotation (gff) files of each reference genome. The putative
216 encoded function of each gene was determined in previous analyses ((for 1A5 see
217 (Plissonneau *et al.* 2018), for 3D7 see (Plissonneau *et al.* 2016)). The annotations were
218 obtained using Interproscan (https://www.ebi.ac.uk/interpro/) against multiple protein
219 databases and then screened using multiple methods (e.g. Signal
220 https://services.healthtech.dtu.dk/service.php?SignalP-5.0, Phobius
221 https://phobius.sbc.su.se/) to determine if the encoded proteins contained likely signal
222 peptides or secreted domains. The putative effect of a SNP in the coding sequence was
223 determined using SNPeff (http://pcingola.github.io/SnpEff/). Pathway (GO and KEGG)
224 enrichment analysis was performed for each trait with a significant QTL that was unique to

225 the KCl environment following a tutorial for non-model species
226 (https://archetypalecology.wordpress.com/2021/01/27/how-to-perform-kegg-and-go-
227 enrichment-analysis-of-non-model-species-using-r/). GO annotations were retrieved from
228 the annotation files describe above. For GO enrichment the R package 'topGo' (Alexa and
229 Rahnenfuhrer 2023) was used to perform a Fischer test on the genes within each QTL
230 interval following the guidelines in the vignette. All three ontologies – Biological Process
231 (BP), Cellular Component (CC) and Molecular Function (MF) were analysed. For KEGG
232 pathways enrichment, GhostKOALA (https://www.kegg.jp/ghostkoala/) was used to find K
233 numbers for all transcripts. The program found K numbers for 34% (4091/11726) and 49%
234 (5970/12072) of transcripts for 3D7 and 1A5 respectively. The enrichment test was
235 performed using the R package clusterProfiler (Wu *et al.* 2021) and the 'enricher' function.
236 The background set for both GO and KEGG was the entire gene/transcript set for each
237 reference genome (3D7 and 1A5).
238
239 **Identifying putative candidate genes in the 3D7x3D1 cross**
240 Genes within a single QTL interval on chromosome 3 were further investigated to identify
241 the most likely candidate genes responsible for the phenotype. We identified the
242 orthologous genes in the 3D1 parent using an analysis performed across the genomes of 19
243 reference strains (Badet *et al.* 2020). We inspected the alignments in the region of interest
244 in IGV. We also blasted the 3D1 gene sequences (including ±200bp flanking regions) against
245 the 3D7 genome to calculate sequence similarity and identify indels.
246
247 **RNAseq data analysis**
248 We analysed RNAseq data that was previously created for the four parental strains during
249 infection of the susceptible wheat cultivar Drifter (Palma-Guerrero *et al.* 2017) as well as
250 cultures grown in vitro on two types of liquid media (yeast sucrose broth (YSB): yeast extract
251 10 g/L and sucrose 10 g/L, pH 6.8; and carbon-depleted minimal medium (MM), pH 5.8
252 (Francisco *et al.* 2019)). The raw sequence reads were downloaded from the Short Read
253 Archive (SRA, https://www.ncbi.nlm.nih.gov/sra, Bioproject: *invitro* SRP152081, *invivo*
254 SRP077418). RNAseq data processing and analysis is described in detail at github
255 (https://github.com/jessstapley/QTL-mapping-Z.-tritici). In brief, reads were trimmed and
256 then mapped to one of two reference genomes (reads from 3D1 and 3D7 were mapped to

257 the 3D7 reference genome while reads from 1E4 and 1A5 were mapped to the 1A5
258 reference genome). Then the number of reads mapping to each gene was counted using
259 R::Rsubread (Liao *et al.* 2019) and we tested for differential gene expression between
260 strains, 3D7 versus 3D1 and 1A5 versus 1E4, using R::EdgeR (Robinson *et al.* 2010).
261
262 **Results**
263 **Effect of KCl on growth and melanisation**
264 A total of 158,480 and 120,059 colonies from the 1A5x1E4 and 3D7x3D1 crosses,
265 respectively, were phenotyped (see Table S2 for details). Differences in growth and
266 melanisation between salt stress and control environments, and growth rate KCl tolerance
267 and melanisation rate KCl tolerance can be seen in Figure 1. We used paired Wilcoxon tests
268 to compare mean trait values between the control and KCl treatments (Table S2). In the
269 presence of KCl, colony radius was smaller at 8 and 12 dpi in both crosses, and the growth
270 rate was reduced in the 3D7x3D1 cross, but not in the 1A5x1E4 cross, suggesting that
271 isolates from the 3D7x3D1 cross were more sensitive to KCl (Figure 1, Table S2). This is
272 consistent with the greater growth rate tolerance in the 1A5x1E4 cross compared to the
273 3D7x3D1 cross ($F_{(1,487)} = 9.19$, p=0.002, growth rate KCl tolerance: 1A5x1E4 = 1.04, 3D7x3D1
274 = 0.96). In the KCl environment we observed less melanisation at both time points and a
275 similar reduced accumulation of melanin over time (melanisation rate) in both crosses
276 (Figure 1, Table S2, $F_{(1,486)} = 2.85$, p=0.09, melanisation rate KCl tolerance: 1A5x1E4 = 0.196,
277 3D7x3D1 = 0.149).
278
279 **Correlations between traits**
280 All pairwise correlations (Pearson, non-parametric) between independent measurements
281 are provided in Tables S3 and S4. Excluding traits that are statistically or functionally
282 coupled, which includes: correlations between two time points of the same trait (e.g. colony
283 radius at 8 dpi and 12 dpi in the control), correlations between a rate and the corresponding
284 time point measurements (e.g. grey value at 12 dpi and melanisation rate in the control), or
285 correlations between rates and KCl tolerance measurements, we identified many
286 correlations between independent measurements (Table S3 and S4). Notably, growth rate in
287 the control environment was correlated with growth rate in the KCl environment in both
288 crosses (r(1A5x1E4) = 0.63 and r(3D7x3D1) = 0.62, Figure S1) – thus isolates that grow faster

289 in a benign environment also grow faster in the presence of salt stress i.e., they have a
290 higher intrinsic growth rate. Melanisation rates showed a similar trend in 1A5x1E4 – isolates
291 that had higher melanisation rates in the benign environment also had higher melanisation
292 rates under KCl stress (Table S4, r = 0.19), but this was not observed in the 3D7x3D1 cross
293 (Table S3, r = 0.07, Figure S1).
294
295 We were particularly interested in the relationship between KCl tolerance and melanisation,
296 as melanin can help protect cells from osmotic stress. In both crosses, the mean grey value
297 in the control environment at 12 dpi was negatively correlated with growth rate KCl
298 tolerance (Tables S2 and S4, 1A5x1E4 r = -0.26 and 3D7x3D1 r = -0.43, Figure S2). The
299 relationship at 8 dpi was also negative in both crosses, but not significant in the 3D7x3D1
300 cross (Tables S3 and S4, 1A5x1E4 r = -0.44 and 3D7x31 r = -0.12, Figure S2). As lower mean
301 grey values correspond to higher amounts of melanin, these correlations indicate that
302 isolates that produce more melanin in a benign environment have a growth rate that is
303 more tolerant to KCl stress, although this relationship was not significant at 8 dpi in the
304 3D7x3D1 cross.
305
306 **QTL results**
307 We identified at least one significant QTL for all traits in the 3D7x2D1 cross and all but four
308 traits (melanisation rate and mean grey value at 12 dpi in the KCl environment, and
309 melanisation rate KCl tolerance at 12dpi, Melanisation rate KCl tolerance) in the 1A5x1E4
310 cross (Table 1). In general, the traits lacking significant QTL had relatively low heritability
311 (Table 1) and thus the power to detect a QTL for those traits was relatively low. All QTL
312 positions, interval sizes and numbers of genes within the interval are presented in Tables 2
313 and 3. Largely overlapping QTL were grouped and given a unique QTL identifier. Examples of
314 how traits measured in different environments can have overlapping QTL intervals are
315 shown in Figure 2. The QTL No. 4, 9 and 11 are each regions of the genome that explain
316 variation in growth rate in both the KCl and control environments. As expected, traits that
317 were highly correlated and/or statistically coupled often had a QTL peak at the same, or
318 overlapping positions (e.g. the 1A5x1E4 grey values in the control environment at 8 dpi and
319 12 dpi mapped to the same position on Chr 2: 1438934bp; the 3D7x3D1 QTL for colony
320 radius at 12 dpi and growth rate in the control environment mapped to Chr 8: 1100862bp).

321 LOD plots for all traits listed in Tables 2 and 3 are provided in the Supplementary Figures S4
322 and Figure S5. In Figures 2 and 3 we provide example plots for only four traits (growth rate
323 in KCl, growth rate in the control, melanisation rate in KCl and melanisation rate in the
324 control) for the two crosses.
325
326 **QTL shared across environments, traits, and time points**
327 Several QTL were shared amongst benign and salt-stress environments, across time points
328 and traits. Only one of these shared QTL is novel to this study, the others were found in
329 earlier studies investigating different stressors. The single novel QTL shared between benign
330 and salt-stress environments was found in the 3D7x3D1 cross on Chr 8 (1100.86-1221.33 Kb,
331 QTL No. 9, Figure 2) and explained variation in seven traits including growth in the control
332 and KCl environments, as well as mean grey value in the control environment and grey value
333 KCl tolerance at 8 dpi (Figure 2, Table 2).
334
335 Of the QTL shared across benign and KCl environments that were identified here and found
336 in earlier studies using different stresses (e.g. cold, fungicide), the most striking – in terms of
337 the number of traits and the magnitude of the LODs, was the QTL on Chr 11 between
338 507.36-658.11 Kb (QTL No. 12) in the 3D7x3D1 cross. This QTL explained variation in 11 of
339 the 18 traits, and in both environments (Table 2). This QTL was identified previously and was
340 found to explain variation in growth, fungicide sensitivity and melanisation in this cross
341 (Lendenmann *et al.* 2014, 2015). The next largest, in terms of number of traits, was a QTL in
342 the 1A5x1E4 cross on Chr 8 between 89.573- 346.224 Kb (QTL No. 10) that explained
343 variation in growth rate, colony radius and grey value in both control and KCl environments
344 (Figure 3, Table 3). This QTL on Chr 8 was also found to explain variation in response to
345 oxidative stress (Zhong *et al.* 2021). Another notable QTL in terms of high LOD (>10) was on
346 Chr 10 (749.521– 1302.645 Kb, QTL No. 10) in the 3D7x3D1 cross, which explained variation
347 in melanisation rate and colony radius in the control environment (Table 2). This QTL was
348 previously found to explain variation in growth-related traits at 10^0C (Lendenmann *et al.*
349 2014) and under oxidative stress (Zhong *et al.* 2021).
350
351 **Unique QTL associated with the KCl environment and pathway enrichment analysis**

352 Several novel QTL that were unique to the KCl environment were also found (indicated with
353 an $^{S\ or\ M}$ in Table 2, 3). In the 3D7x3D1 cross, two QTL were found for traits related to colony
354 radius: the first on Chr 3 (QTL No. 3) explained variation in colony radius in KCl at 8 dpi and
355 colony radius KCl tolerance at 8 and 12 dpi; and the second on Chr 4 (QTL No. 5) explained
356 variation in colony radius in KCl at 8 dpi and colony radius KCl tolerance at 8 dpi. For
357 melanin-related traits, four QTL were found in the 3D7x3D1 cross: the first on Chr 1 (QTL
358 No. 1) explained variation in three traits (melanisation rate in KCl, melanisation rate KCl
359 tolerance and grey value in KCL at 12 dpi); the second on Chr 2 (QTL No. 2) explained
360 variation in grey value in KCl at 12 dpi; the third on Chr 6 (QTL No. 6) explained variation in
361 melanisation rate in KCl; and the fourth on Chr 8 (QTL No. 8) explained variation in grey
362 value in KCl at 8 dpi. In the 1A5x1E4 cross a total of three QTL related to colony radius in KCl
363 were found. The first was on Chr 1: QTL No. 2 explained variation in colony radius KCl
364 tolerance at 12 dpi, growth rate KCl tolerance, and colony radius in KCl at 12 dpi. The second
365 unique KCl environment QTL was on Chr 5 (QTL No. 7) and explained variation in growth
366 rate KCl tolerance; the fifth on Chr 6 (QTL No. 8) explained variation in radius at 8 dpi in KCl.
367 No unique QTL were found for melanin-related traits in the 1A5x1E4 cross.
368
369 For pathway enrichment analyses we focussed on traits that had significant QTLs unique to
370 the KCl environment (indicated in Tables 2 and 3 with $^{S\ or\ M}$) and investigated if genes
371 associated with those traits were enriched for KEGG pathways or GO annotations. We
372 analysed each trait-QTL separately and did the same analysis using all genes for size- or
373 melanin-related traits combined (Table S5, Table S6). No significantly enriched KEGG
374 pathways were identified in our data. For the GO enrichment we report on the results for
375 size- or melanin-related trait-QTL combined and we use the raw p-values instead of the
376 adjusted p-values as indicators of possible GO enrichment because adjusting p-values in GO
377 enrichment analysis may be too conservative and inappropriate (Alexa and Rahnenfuhrer
378 2023). All results are presented in Supplementary Tables S5 and S6. Considering all genes
379 within size-related unique KCl QTL combined in the 3D7x3D1 cross (Table 2, QTL No.^{S}): for
380 Biological Process (BP) double-strand break repair via nonhomologous end joining
381 (GO:0006303) and nucleotide-excision repair (GO:0006289) GO terms were enriched; for
382 Cellular Component (CC) Ku70:Ku80 complex (GO:0043564) GO term was enriched; and for
383 Molecular Function (MF) GTPase activity (GO:0003924), superoxide dismutase activity

384 (GO:0004784), telomeric DNA binding (GO:0042162) and damaged DNA binding
385 (GO:0003684) GO terms were enriched (Table S5b). There were 15 genes within these QTLs
386 that have one or more of these GO annotations (Table S7a). For genes within melanin-
387 related unique KCl QTL combined in the 3D7x3D1 cross (Table 2 QTL No.^{M}): for BP
388 glutathione biosynthetic process (GO:0006750) GO terms was enriched; for CC no GO term
389 was enriched; and for MF chaperone binding (GO:0051087), phosphatidylinositol
390 phospholipase C activity (GO:0004435), and shikimate 3-dehydrogenase (NADP+) activity
391 (GO:0004764) GO terms were enriched (Table S5d). There were 13 genes within these QTLs
392 that have one or more of these GO annotations (Table S7b). Considering all genes within
393 size-related unique KCl QTL combined in the 1A5x1E4 cross (Table 2 QTL No.^{S}): for BP no GO
394 terms were enriched; for CC cell wall (GO:0005618) GO term was enriched; and for MF
395 chaperone binding (GO:0051087) and triglyceride lipase activity (GO:0004806) GO terms
396 were enriched (Table S6b). There were 12 genes within these QTLs that have one or more of
397 these GO annotations (Table S7c). There were no unique KCl melanin-related QTL in the
398 1A5x1E4 cross.
399
400 **Analysis of QTL No. 3 in 3D7x3D1 and identification of candidate genes**
401 To identify candidate genes associated with KCl stress, we focused attention on novel QTL
402 with a high LOD (>10), relatively narrow intervals, and that explained a relatively high
403 proportion of the variation for a KCl-associated trait. Only QTL No. 3 in the 3D7x3D1 cross
404 met these requirements (Table 2). This QTL had a high LOD (>10) for colony radius at 8 dpi in
405 the KCl environment and colony radius KCl tolerance at 8 dpi. The LOD peaked at 22.8 at
406 chromosome position 737773 bp. This QTL explained 33% of the phenotypic variance in
407 colony radius at 8 dpi and 23% of the variance in colony radius KCl tolerance at 8 dpi.
408 Isolates with the non-reference allele at the QTL peak marker had larger colonies at 8 dpi
409 (F=113.1, df=1,233, p=<0.001, Figure 4c) and greater colony radius KCl tolerance at 8 dpi
410 (F=56.07, df=1,23, p=<0.001). The Bayes confidence interval for the QTL for colony radius in
411 KCl at 8 dpi spanned 149.29 Kb and contained 94 SNPs and 36 genes (Table 2, Figure 4b). For
412 this interval we present data on the genes in the reference genome (3D7), the orthologous
413 genes in 3D1, the gene sequence similarity (including ±200bp of flanking regions) between
414 the parents, the gene's putative encoded function (PFAM database) and if there is any

415 evidence of differential gene expression between the parents across all available datasets
416 (Table 4 and see Table S8 for full details).
417
418 Several genes had SNP variation predicted to have a high impact based on SNPEff analysis
419 (Table S9, *ZT3D7_G3622*, *ZT3D7_G3623*, *ZT3D7_G3624, ZT3D7_G3632, ZT3D7_G3633,*
420 *ZT3D7_G3635, ZT3D7_G3649*). A transposable element (6927 bp) was found within 200 bp
421 of *ZT3D7_G3623*, and one gene, *ZT3D7_G3649* is a singleton – with no orthologue present
422 in any of the other 18 *Z. tritici* reference genome sequences (Table S8). Two genes within
423 this QTL interval and another gene immediately adjacent to the interval have GO
424 annotations that were enriched (ZT3D7_G3648, ZT3D7_G3652, ZT3D7_G3659, Table S7).
425 ZT3D7_G3648 and ZT3D7_G3659 have predicted GTPase activity (GO:0003924) and
426 ZT3D7_G3652 has predicted superoxide dismutase activity (GO:0004784). The SNP variation
427 in these genes between the parents was not predicted to have a large impact on the protein
428 (Table S9). Based on predicted protein function, and sequence and gene expression
429 variation between the parents, we consider six genes to be the most promising candidates
430 for further analyses: *ZT3D7_G3622*, *ZT3D7_G3635*, *ZT3D7_G3637*, *ZT3D7_G3639*,
431 *ZT3D7_G3655* and *ZT3D7_G3658* (this order reflects their relative positions on chromosome
432 3).
433
434 *ZT3D7_G3622* has a loss of function SNP (Chr 3:598092) in 3D1 that is predicted to cause a
435 loss of a predicted start codon. The gene contains a single exon, encodes a protein length of
436 550 amino acids (aa) and is predicted to contain a fungal-specific transcription factor
437 domain and Zn(2)-C6 fungal-type DNA-binding domain (Table 4). The orthologue in the 3D1
438 genome is *ZT3D1_G3567*. It encodes a longer protein (722 aa) and has two exons, the first
439 exon's product encodes a Zn(2)-C6 fungal-type DNA-binding domain and the second exon's
440 product is the same as that of *ZT3D7_G3622*. The predicted protein in 3D1 is the same as
441 the orthologue in IPO323 (*Mycgr3T108446*). Although we do have reads mapping to this
442 region, and when grown in vitro on MM this gene is downregulated in 3D1 compared to 3D7
443 (Table S8), our RNA sequence data does not clearly support gene models in either 3D1 or
444 3D7, there are no clear exon/intron boundaries. This suggests that the annotation of this
445 gene may require manual curation.
446

447 *ZT3D7_G3635* has a high impact SNP variant (Chr 3:681906) that is predicted to cause a
448 frameshift. The gene has 6 exons in 3D7 and encodes a protein length of 1078 aa. Based on
449 INTERPROSCAN and Ensemble Fungi, the protein has multiple predicted domains; the
450 largest is a protein kinase domain. The protein also contains a Serine/threonine-protein
451 kinase active site and the molecular function of the first GO term (GO:0004674) is protein
452 serine/threonine kinase activity – suggesting that this gene is likely to be involved in osmotic
453 stress response (Hohmann 2002). The RNA sequence data supports the gene model. The
454 orthologue in 3D1 is *ZT3D1_G3580*, which has 3 exons and multiple predicted domains that
455 do not differ from those predicted for *ZT3D7_G3635*. The gene is up-regulated in vitro on
456 YSB and down-regulated in planta at 28d in 3D1 compared to 3D7 (Table S8).
457
458 *ZT3D7_G3637* has one exon, encodes a protein length of 1285 aa, and includes multiple
459 predicted domains including a DEAD/DEAH box helicase, which is involved in plant
460 responses to osmotic stress (Nguyen *et al.* 2018). The orthologue in 3D1 (*ZT3D1_G3583*)
461 encodes a similar protein as *ZT3D7_G3637* – has the same length and has the same
462 predicted domains. There are no high impact SNPs between the parents, but several
463 moderate and low impact variants were identified (Table S*). The RNA sequence data
464 supports the annotation, and the gene is down regulated in 3D1 in both YSB and MM (Table
465 S8).
466
467 *ZT3D7_G3639* has 4 exons in 3D7. The gene sequence similarity between 3D7 and 3D1 is
468 98.66% and there is an 8 bp intronic deletion in 3D1. This gene belongs to the Major
469 Facilitator Superfamily (MFS) and encodes a protein length of 512 aa. According to the
470 Phobius analysis, the gene contains 12 transmembrane segments (Table S8). Proteins with
471 transmembrane activity and transmembrane segments are likely to play an important role
472 in sensing and regulating osmotic stress (Hohmann 2002). The orthologue in 3D1 is
473 *ZT3D1_G3580*, which has the same number of exons, encodes the same protein length and
474 has the same predicted function. The RNA sequence data supports the gene model, and the
475 differential expression analysis found the gene is downregulated in planta at 12 and 14 days
476 in 3D1 compared to 3D7 (Table S8).
477

478 *ZT3D7_G3655* has one exon and encodes a protein length of 848 aa. The gene contains 10
479 transmembrane segments (Table S8) and encodes a voltage-gated chloride channel domain
480 – thus it is likely to be involved in osmotic stress responses. The gene sequence between the
481 parents is almost identical, but there is one moderate effect SNP within the gene (Table S9).
482 When grown in vitro on MM this gene is upregulated in 3D1 compared to 3D7. The RNA
483 sequence data supports the gene model annotation.
484
485 *ZT3D7_G3658* has four exons and encodes a protein length of 614 aa. Its orthologue in 3D1
486 (*ZT3D1_G3604*) has three exons and encodes 572 aa. The gene encodes a vacuolar protein
487 sorting-associated protein 17, Vps17. Vacuoles play an important role in osmotic stress
488 responses: their fission and fusion enable cells to maintain turgor pressure and regulate cell
489 volume (Richards *et al.* 2010). Comparison of the 3D1 gene sequence to the 3D7 genome
490 using BLAST revealed that the 3D7 gene sequence was identical, but the 3D1 orthologue
491 annotation is shorter and has only three exons. Our RNA sequence data supports the 3D1
492 annotation with only 3 exons, as there were no RNA sequence reads mapping to exon 1 of
493 the *ZT3D7_G36580*. This gene was downregulated in vitro in both MM and YSB in 3D1
494 compared to 3D7.
495
496 **4. Discussion**
497 We were able to map major effect loci affecting colony growth and melanisation in the
498 presence of potassium chloride in both crosses. We focussed on QTL that were unique to
499 the KCl environment to identify candidate genes that are specific to osmotic stress – as
500 opposed to finding genes that may be more generally related to intrinsic growth or melanin
501 production. A QTL on Chr 3 in the 3D7x3D1 cross was the most promising for identifying
502 genes specifically associated with KCl stress. We highlighted the six most promising
503 candidate genes in this QTL based on their predicted encoded functions, sequence similarity
504 and transcriptional profiles. We also identified several QTL shared across environments and
505 confirmed that several previously identified QTL, which explained variation in growth and
506 melanisation across different environmental stressors (Table 2 and 3, e.g. 3D7x3D1 Chr 11
507 and 1A5x1E4 Chr 8), also explained trait variation in the presence of osmotic stress.
508
509 **Effect of KCl on colonies**

510 In the presence of potassium chloride at 0.75M, colonies were typically smaller and less
511 melanised compared to the control environment (Figure 1, Table S2). A reduction in colony
512 radius in the KCl environment supports our hypothesis that this environment was stressful
513 to *Z. tritici*. Our results suggest that growth rate in the 1A5x1E4 cross was less affected by
514 KCl-induced osmotic stress, as mean growth rate was not reduced in the KCl environment,
515 compared to the 3D7x3D1 cross that exhibited a significantly reduced growth rate (Table
516 S2). However, we note that the overall difference in growth rate in the 3D7x3D1 progeny
517 between the control and KCl environments was relatively small (~6% reduction in growth,
518 Table S2).
519
520 When experiencing osmotic stress, an increase in melanin is thought to protect cells by
521 strengthening the fungal cell wall, but a reduced metabolic capacity under stress may limit
522 the ability of a cell to produce melanin. The mean colony grey values were higher, indicative
523 of lower levels of melanin, for strains grown in the KCl environment (Table S2). This suggests
524 that the *Z. tritici* response to osmotic stress did not involve an increased production of
525 melanin to protect the cells as was observed in halotolerant species (Kogej *et al.* 2007). We
526 did observe however, that isolates that were more melanised in the benign control
527 environment (lower Grey Value) were more tolerant to salt stress (Figure S2) – their growth
528 rates were higher and their reductions in melanisation were lower compared to isolates that
529 were less melanised in the control environment (Table S3, S4). This suggests that strains
530 having a greater intrinsic capacity to become melanised are more tolerant to salt stress.
531
532 **Shared QTL**
533 Some QTL that explained variation in growth and melanisation in the stressful environment
534 overlapped with QTL for trait variation in the control environment. Prominent examples
535 include the Chr 11 QTL No. 11 in the 3D7x3D1 cross and the Chr 8 QTL No. 10 in the
536 1A5x1E4 cross. These genomic regions may harbour genes that affect intrinsic growth of
537 colonies under a wide range of environments and/or genes with pleiotropic effects. Many of
538 the QTL shared across environments were identified in earlier experiments and discussed
539 previously (Lendenmann *et al.* 2015; Zhong *et al.* 2021). The QTL No. 11 in the 3D7x3D1 was
540 shown to be due to differential expression of the *Zmr1* gene encoding a transcription factor
541 that regulates synthesis of DHN melanin in *Z. tritici* (Krishnan et al. 2018). *Zmr1* was shown

542 to have pleiotropic effects on melanin production, colony growth rates and fungicide
543 resistance (Krishnan et al. 2018).
544
545 **QTL uniquely associated with the KCl environment**
546 This QTL analysis enabled us to identity large effect loci that explain variation in traits under
547 KCl stress. Among the QTL uniquely associated with KCl stress, most had moderate LODs
548 with each QTL explaining only a small proportion of the phenotypic variance (3D7x3D1
549 maximum = 0.10, 1A5x1E4 maximum = 0.11). The exception was QTL No. 3 in the 3D7x3D1
550 cross, which explained up to 33% of the phenotypic variance. This QTL on chromosome 3
551 was associated with differences in colony radius at 8 dpi and colony radius KCl tolerance at 8
552 and 12 dpi. We targeted this QTL for further investigation, seeking to identify genes
553 specifically associated with KCl tolerance. It is interesting to note that no LOD peak was
554 detected for colony radius at 12 dpi, even though colony radius at 12 dpi was correlated
555 with colony radius at 8 dpi (Table S4, correlation = 0.58, $p<0.001$). As growth rate is based
556 on the change in colony radius between 8 and 12 dpi, we might expect growth rate in KCl to
557 share the QTL for colony radius at 8 dpi. To better understand why growth rate does not
558 share this QTL, we examined the trait correlations. Growth rate is highly correlated with
559 colony radius at 12 dpi (0.93) and less strongly correlated with colony radius at 8 dpi (0.26)
560 (Table S4). There is less variation in colony radius at 8 dpi, thus colony radius at 12 dpi has a
561 greater impact on the growth rate. The QTL No. 3 also explained variation in colony radius
562 KCl tolerance at 8 and 12 dpi, although the association with this trait at 12 dpi explained
563 relatively little phenotypic variation (0.08). Thus, the QTL peak is more strongly associated
564 with colony radius and colony radius KCl tolerance at an earlier stage of colony growth. A
565 similar pattern was observed in the chromosome 11 QTL associated with melanisation
566 (Lendenmann *et al.* 2014; Krishnan *et al.* 2018), with the QTL LOD score very high in the
567 younger colonies and decreasing as colonies aged. After cloning and characterizing the *Zmr1*
568 gene and its functions, this pattern could be explained based on the finding that the
569 difference in *Zmr1* expression (and the resulting difference in melanisation) was significantly
570 higher in younger colonies than in older colonies (Krishnan *et al.* 2018). We hypothesize that
571 QTL no. 3 associated with KCl tolerance is underpinned by a similar mechanism that is
572 specific to the earlier stage of colony growth.
573

574 **Candidate genes in the QTL for colony radius and colony radius KCl tolerance at 8 dpi in**
575 **the 3D7x3D1 cross**
576 Among the 36 genes found in the interval spanning this QTL No. 3, we consider six genes to
577 be the most promising candidates to be involved in sensing and responding to salt stress
578 and responsible for this QTL. Below we consider each in turn in the order of their relative
579 positions on chromosome 3.
580
581 The first candidate gene, *ZT3D7_G3622*, is predicted to encode a fungal-specific
582 transcription factor. The orthologue in the IPO323 reference genome (assembly MYCGR
583 v2.0) is *Mycgr3T108446* and it has 21 paralogs. Transcription factors (TFs) regulate gene
584 expression and are important regulators of molecular responses to environmental stimuli
585 (e.g. Hohmann, 2002; Shi et al., 2021), making this gene a good candidate. The *Zmr1* gene
586 identified in this same cross and shown to be responsible for differences in melanisation,
587 with greater effects in younger colonies, is a transcription factor (Krishnan et al. 2018). The
588 SNP variant in 3D1 (Chr 3:598092) is predicted to cause a loss of the start codon that is likely
589 to cause a loss of function. In *F. graminearum,* mutants lacking a similar TF (called *Fss1*)
590 were sensitive to high sodium and lithium, but they were not sensitive to elevated
591 potassium (Son *et al.* 2015).
592
593 The second candidate, *ZT3D7_G3635* is predicted to encode a serine/threonine-protein
594 kinase active site, which is known to regulate MAP kinases (Hohmann 2002; Li *et al.* 2019). A
595 SNP variant found in the 3D1 allele is predicted to cause a frameshift that is likely to cause a
596 loss of function. The ortholog in the IPO323 genome is *Mycgr3G56270* and it has one
597 paralog in the reference genome. A serine/threonine kinase from *Aspergillus flavus*,
598 *AflSte20*, was recently functionally validated using a knockout mutant. This study showed
599 that the knockout had higher sensitivity to osmotic stress compared to the wild type (Li *et*
600 *al.* 2019), confirming the role of this serine/threonine-protein kinase in osmotic stress
601 response in a different fungal plant pathogen.
602
603 The third candidate, *ZT3D7_G3637* is predicted to encode a DEAD/DEAH box helicase
604 domain. The reference genome orthologue is *Mycgr3G99415* and it has 6 paralogs. The
605 DEAD – box helicases are the largest RNA helicase (RH) subfamily. In plants they play

606 multiple functional roles and are important in stress responses (Pandey *et al.* 2020). For
607 example, in *Arabidopsis thaliana AtRH17* is involved in salt-stress tolerance (Nguyen *et al.*
608 2018), in rice *OsABP* is upregulated in response to salt (Macovei *et al.* 2012) and in barley
609 HvD1 accumulated in salt- and cold-stressed plants (Nakamura *et al.* 2004). In wheat, the
610 DEAD-box helicase *TaRH1* that was first identified as a component of the defence response
611 to stripe rust (*Puccinia striiformis f*. sp. *tritici*) was also found to be involved in plant
612 response to multiple stressors, including salt stress (Zhang *et al.* 2014). SNP variation found
613 between the parents was predicted to have only moderate effects, no high impact SNPs
614 were detected. We chose this gene as a promising candidate based mainly on its known
615 associations with salt stress in plants and the significant differences in expression found
616 between 3D1 and 3D7 while growing in vitro.
617
618 A gene encoding a Major Facilitator Superfamily (MFS) domain, *ZT3D7_G3639* is the fourth
619 candidate we highlight. The reference genome orthologue is *Mycgr3G85019* and it has 58
620 paralogs. MFS transporters facilitate the movement of small solutes across cell membranes
621 in response to chemiosmotic gradients – making them likely to play an important role in
622 sensing and regulating osmotic stress (Hohmann 2002). We chose this gene as a promising
623 candidate based mainly on its known functions and associations with multiple stressors
624 including fungicides (Dos Santos *et al.* 2014; Omrane *et al.* 2015).
625
626 The fifth highlighted gene is *ZT3D7_G3655* that encodes a voltage gated chloride channel
627 domain and membrane transport domains. The reference genome orthologue is
628 *Mycgr3T20761* and there are three paralogues in the IPO323 reference genome. Chloride
629 channels are important in animal cell volume regulation (Jentsch *et al.* 2002), fungal
630 oxidative stress response (Oddon *et al.* 2007), fungal pathogen virulence (Zhu and
631 Williamson 2003; Cañero and Roncero 2008) and plant immunity (Guo *et al.* 2014). The role
632 of chloride channels in response to salt stress is well established in animals (Jentsch *et al.*
633 2002), and to a lesser degree in plants (Barbier-Brygoo *et al.* 2011), but less is known from
634 fungi. For one of the better-known families of chloride channels, the CLC family, a single
635 gene (*GEF1*) has been identified in yeast. In two pathogenic fungi (*Cryptococcus neoformans*
636 and *Fusarium oxysporum*) – the GEF1 homologue has been shown to influence virulence
637 (Zhu and Williamson 2003; Cañero and Roncero 2008). The gene sequence between the

638 parents is highly conserved, however gene expression differences were observed in minimal
639 media, so differences may exist in the regulatory sequence.
640
641 The final candidate we highlight is *ZT3D7_G3658*, which encodes a Vacuolar associated
642 protein 17, *Vps17*. The orthologous gene in the reference genome is *Mycgr3T108464* and
643 there are six paralogues. Comparing the DNA sequence of this gene against the 3D1 genome
644 revealed an identical sequence, but the annotation of the gene in 3D7 and 3D1 differs – the
645 3D1 orthologue protein length is shorter and the gene has one fewer exons. Our RNA
646 sequence data suggests that the *ZT3D7_G3658* annotation may be incorrect - there were no
647 reads mapping to the first, small exon of this gene. This suggests that the annotation of this
648 gene may need manual curation before conducting further analyses. The gene was
649 downregulated in YSB and MM in 3D1 compared to 3D7, demonstrating that transcription
650 of this gene varies between the parents. Vacuoles play important roles in both osmotic
651 stress responses (Richards *et al.* 2010) and virulence (Li *et al.* 2021). Under salt stress the
652 vacuoles can undergo fusion and fission – changing in size and number (Richards *et al.*
653 2010). *Vsp17* knockouts in *S. cerevisiae* had many small vacuoles but were resistant to
654 osmotic stress and could sporulate (Köhrer and Emr 1993). We are unaware of any work
655 that has investigated the role of *Vsp17* in salt-stress responses of filamentous fungi.
656
657 **Enrichment analysis of QTL unique to the KCl environment**
658 We investigated if genes within QTL unique to the KCl environment were functionally
659 enriched. We considered each cross separately and considered colony size-related traits and
660 melanin-related traits separately (Table 2, 3: QTL No.$^{S\ or\ M}$). No KEGG pathway enrichment
661 was detected. This may reflect the relatively low number of genes that were assigned a K
662 number (3D7 34%, 1A5 49%). The GO enrichment analysis provided some interesting
663 results. For QTL associated with colony size related traits, two notable GO annotations were
664 enriched. The first was cell wall (GO:0005618) which was enriched in QTLs in the 1A5x1E4
665 cross. Cell wall remodelling is an important response to osmotic stress and this remodelling
666 is mediated by the Hog1 and MAPK pathways (as described earlier). The cell wall GO is
667 associated with four genes in the QTL intervals: ZT1A5_G201, ZT1A5_G1063, ZT1A5_G1074,
668 and ZT1A5_G1774. A common annotation feature of the first two genes is they contain a
669 glycoside hydrolase family 16, which is involved in degradation and remodelling of the cell

670 wall. In rice blast (*M. oryzae*), glycoside hydrolases II homolog (MoGls2) mutants showed
671 defects in cell wall integrity, were less sensitive to salt stress and had reduced virulence (Li
672 *et al.* 2016). The other two genes with this GO term (ZT1A5_G1074, ZT1A5_G1774) contain
673 yeast PIR protein repeat. A number of yeast cell wall glycoproteins are characterised by the
674 presence of internal repeats (PIR, tandem repeats of 18 to 19 amino acid residues) and
675 these are important in yeast response to multiple environmental stressors and antifungal
676 agents (Mazáň *et al.* 2008). The second notable GO enrichment was for GO terms related to
677 DNA repair (GO:0006281: nucleotide-excision repair, double-strand break repair via
678 nonhomologous end joining). DNA repair genes can be upregulated in the presence of a
679 variety of environmental stressors and are widely considered an important response to
680 stress (Hohmann 2002). Six genes have these GO annotations (ZT3D7_G5293,
681 ZT3D7_G3673, ZT3D7_G3591, ZT3D7_G5301, ZT3D7_G5305, ZT3D7_G5361). Three of these
682 genes (ZT3D7_G5293, ZT3D7_G3673, ZT3D7_G53601) have multiple GO annotations, of
683 which three were also enriched: DNA binding (GO:0043564), damaged DNA binding
684 (GO:0003684), and telomeric DNA binding (GO:0042162). Another three genes with
685 enriched GO annotations were in or adjacent to the large LOD QTL on chromosome 3
686 (Figure 4, Table 4) in the 3D7x3D1 cross (ZT3D7_G3648, ZT3D7_G3652, ZT3D7_G3659, Table
687 S7). Two have predicted GTPase activity (GO:0003924, ZT3D7_G3648 and ZT3D7_G3659).
688 GTPase are involved in many functions in fungi, including during plant-fungal interactions. A
689 well-studied GTPase family, *Ras*, has been shown to be involved in response to osmotic
690 stress in *Beauveria bassiana* and *Botrytis cinerea* (Dautt-Castro *et al.* 2021). Fungal
691 treatments targeting Ras proteins are being tested to control human pathogens with
692 promising results (LeBlanc *et al.* 2020). The other gene in the interval, ZT3D7_G3652 has
693 predicted superoxide dismutase activity (GO:0004784). Genes in this family are known to
694 play an important role in defending cells against reactive oxygen species, and in the stripe
695 rust fungus (*Puccinia striiformis* f. sp. *Tritici*) this can help guard against plant defences and
696 facilitate infection (Zheng *et al.* 2020).
697
698 There was also a notable GO term enriched for melanin-related QTL: glutathione
699 biosynthetic process (GO:0006750). This GO term was associated with three genes within
700 QTLs: ZT3D7_G1409, ZT3D7_G1830, ZT3D7_G8325. Glutathione is a metabolite that plays a
701 major role in response to stress, morphogenesis, and virulence in fungi (Wangsanut and

702 Pongpom 2022). In *Cryptococcus neoformans,* a glutathione gene mutant (gsh2Δ) had
703 increased sensitivity to salt (Berndt and Lillig 2017), and *Schizosaccharomyces pombe* grown
704 in vitro under multiple stressors, including osmotic stress, had increased expression of the
705 glutathione reductase gene (*pgr1*) (Lee *et al.* 1997). Our results suggest that glutathione
706 may also be important in osmotic stress response in *Z. tritici*. All the genes highlighted in our
707 GO enrichment analysis may be useful targets for further investigation to understand the
708 molecular response of *Z. tritici* to salt stress, but may also provide interesting targets for
709 fungicide development.
710
711 **QTL reproducibility**
712 This dataset allowed us to explore the repeatability of previously identified QTL from other
713 published datasets. One earlier dataset used the same mapping populations but different
714 experimental conditions and treatments, with a different reference genome and different
715 genetic markers and map information (Lendenmann et al., 2015, 2014). A second earlier
716 dataset used the same isolates and experimental conditions, but different treatments and
717 different marker and map information (Zhong *et al.* 2021). Comparisons across these three
718 data sets yielded several consistent QTL. Our analyses confirmed that a region on
719 chromosome 11 in the 3D7x3D1 cross (Table 2, QTL No. 11) is associated with variation in
720 melanisation and growth in multiple environments (e.g. under fungicide stress in
721 Lendenmann et al., 2015; under oxidative stress in Zhong et al., 2021). This QTL contains the
722 *Zmr1* transcription factor that was shown to regulate melanin production (Krishnan *et al.*
723 2018). We hypothesize that *Zmr1* also explains the variation we observed under salt-stress.
724 A QTL associated with multiple growth and melanin traits in the 1A5x1E4 cross on
725 chromosome 8 (Table 3, QTL No. 13) overlaps with a previously identified QTL on
726 chromosome 8 that was associated with colony growth and tolerance to oxidative stress
727 (Zhong *et al.* 2021). These findings illustrate that many of our QTL are reproducible across
728 experiments and increases our confidence that we have identified biologically meaningful
729 genomic regions using our automated image analyses.
730
731 **Authorship contribution statement**

Jessica Stapley: Formal analysis, Data curation, Writing - Original Draft, Writing - Review & Editing, Resources, Data curation. Bruce A. McDonald: Conceptualization, Methodology, Writing - Review & Editing, Supervision, Project administration, Funding acquisition.

Declaration of Competing Interest

The authors declare that they have no known competing financial interests or personal relationships that could have appeared to influence the work reported in this paper

Data availability

Phenotypic and SNP data are available at ETH Data repository (DOI: 10.3929/ethz-b-000550424). All code and details of the analysis are available at (https://github.com/jessstapley/QTL-mapping-Z.-tritici).

Acknowledgments

We thank Ziming Zhong, Tiziana Valeria Vonlanthen, Bethan Turnbull, Susanne Dora, Sarah Furler, Alexandra Waltenspühl, and Jasmin Wiedmer for collecting the phenotypic data and Javier Palma-Guerrero for supervision. We thank Marcello Zala for assistance in the laboratory. This research was supported by the Swiss National Science Foundation (31003A_155955 granted to BAM).

753 **References**

754 Alexa A., and J. Rahnenfuhrer, 2023 Topgo: enrichment analysis for gene ontology.

755 Araújo C. A. S., P. C. Ferreira, B. Pupin, L. P. Dias, J. Avalos, *et al.*, 2020 Osmotolerance as a
756 determinant of microbial ecology: A study of phylogenetically diverse fungi. Fungal
757 Biol. 124: 273–288. https://doi.org/10.1016/j.funbio.2019.09.001

758 Badet T., U. Oggenfuss, L. Abraham, B. A. McDonald, and D. Croll, 2020 A 19-isolate
759 reference-quality global pangenome for the fungal wheat pathogen *Zymoseptoria*
760 *tritici*. BMC Biol. 18: 12. https://doi.org/10.1186/s12915-020-0744-3

761 Barbier-Brygoo H., A. De Angeli, S. Filleur, J.-M. Frachisse, F. Gambale, *et al.*, 2011 Anion
762 channels/transporters in plants: from molecular bases to regulatory networks. Annu.
763 Rev. Plant Biol. 62: 25–51. https://doi.org/10.1146/annurev-arplant-042110-103741

764 Berndt C., and C. H. Lillig, 2017 Glutathione, Glutaredoxins, and Iron. Antioxid. Redox Signal.
765 27: 1235–1251. https://doi.org/10.1089/ars.2017.7132

766 Broman K. W., H. Wu, S. Sen, and G. A. Churchill, 2003 R/qtl: QTL mapping in experimental
767 crosses. Bioinformatics 19: 889–890. https://doi.org/10.1093/bioinformatics/btg112

768 Cañero D. C., and M. I. G. Roncero, 2008 Influence of the chloride channel of *Fusarium*
769 *oxysporum* on extracellular laccase activity and virulence on tomato plants.
770 Microbiology 154: 1474–1481. https://doi.org/10.1099/mic.0.2007/015388-0

771 Croll D., M. Zala, and B. A. McDonald, 2013 Breakage-fusion-bridge cycles and large
772 insertions contribute to the rapid evolution of accessory chromosomes in a fungal
773 pathogen. PLOS Genet. 9: e1003567. https://doi.org/10.1371/journal.pgen.1003567

774 Dautt-Castro M., M. Rosendo-Vargas, and S. Casas-Flores, 2021 The Small GTPases in Fungal
775 Signaling Conservation and Function. Cells 10: 1039.
776 https://doi.org/10.3390/cells10051039

777 Dos Santos S. C., M. C. Teixeira, P. J. Dias, and I. Sá-Correia, 2014 MFS transporters required
778 for multidrug/multixenobiotic (MD/MX) resistance in the model yeast:
779 understanding their physiological function through post-genomic approaches. Front.
780 Physiol. 5: 180–180. https://doi.org/10.3389/fphys.2014.00180

781 Duran R., J. W. Cary, and A. M. Calvo, 2010 Role of the osmotic stress regulatory pathway in
782 morphogenesis and secondary metabolism in filamentous fungi. Toxins 2: 367–381.
783 https://doi.org/10.3390/toxins2040367

784 Francisco C. S., X. Ma, M. M. Zwyssig, B. A. McDonald, and J. Palma-Guerrero, 2019
785 Morphological changes in response to environmental stresses in the fungal plant
786 pathogen *Zymoseptoria tritici*. Sci. Rep. 9: 9642. https://doi.org/10.1038/s41598-
787 019-45994-3

788 Francisco C. S., B. A. McDonald, and J. Palma-Guerrero, 2023 A transcription factor and a
789 phosphatase regulate temperature-dependent morphogenesis in the fungal plant
790 pathogen Zymoseptoria tritici. Fungal Genet. Biol. 167: 103811.
791 https://doi.org/10.1016/j.fgb.2023.103811

792 Guo W., Z. Zuo, X. Cheng, J. Sun, H. Li, *et al.*, 2014 The chloride channel family gene CLCd
793 negatively regulates pathogen-associated molecular pattern (PAMP)-triggered
794 immunity in Arabidopsis. J. Exp. Bot. 65: 1205–1215.
795 https://doi.org/10.1093/jxb/ert484

796 Hohmann S., 2002 Osmotic stress signaling and osmoadaptation in yeasts. Microbiol. Mol.
797 Biol. Rev. 66: 300–372. https://doi.org/10.1128/MMBR.66.2.300-372.2002

798 Jacob S., A. J. Foster, A. Yemelin, and E. Thines, 2015 High osmolarity glycerol (HOG)
799 signalling in *Magnaporthe oryzae*: Identification of MoYPD1 and its role in
800 osmoregulation, fungicide action, and pathogenicity. Fungal Biol. 119: 580–594.
801 https://doi.org/10.1016/j.funbio.2015.03.003

802 Jentsch T. J., V. Stein, F. Weinreich, and A. A. Zdebik, 2002 Molecular structure and
803 physiological function of chloride channels. Physiol. Rev. 82: 503–568.
804 https://doi.org/10.1152/physrev.00029.2001

805 Jiang C., G. Lv, J. Ge, B. He, Z. Zhang, *et al.*, 2021 Genome-wide identification of the GATA
806 transcription factor family and their expression patterns under temperature and salt
807 stress in *Aspergillus oryzae*. AMB Express 11: 56. https://doi.org/10.1186/s13568-
808 021-01212-w

809 Kogej T., M. Stein, M. Volkmann, A. A. Gorbushina, E. A. Galinski, *et al.*, 2007 Osmotic
810 adaptation of the halophilic fungus *Hortaea werneckii*: role of osmolytes and
811 melanization. Microbiology 153: 4261–4273.
812 https://doi.org/10.1099/mic.0.2007/010751-0

813 Köhrer K., and S. Emr, 1993 The yeast VPS17 gene encodes a membrane-associated protein
814 required for the sorting of soluble vacuolar hydrolases. J. Biol. Chem. 268: 559—569.
815 https://doi.org/10.1016/s0021-9258(18)54188-0

816 Krishnan P., L. Meile, C. Plissonneau, X. Ma, F. E. Hartmann, *et al.*, 2018 Transposable
817 element insertions shape gene regulation and melanin production in a fungal
818 pathogen of wheat. BMC Biol. 16: 78. https://doi.org/10.1186/s12915-018-0543-2

819 LeBlanc E. V., E. J. Polvi, A. O. Veri, G. G. Privé, and L. E. Cowen, 2020 Structure-guided
820 approaches to targeting stress responses in human fungal pathogens. J. Biol. Chem.
821 295: 14458–14472. https://doi.org/10.1074/jbc.REV120.013731

822 Lee J., I. W. Dawes, and J.-H. Roe, 1997 Isolation, Expression, and Regulation of thepgr1 +
823 Gene Encoding Glutathione Reductase Absolutely Required for the Growth of
824 Schizosaccharomyces pombe. J. Biol. Chem. 272: 23042–23049.
825 https://doi.org/10.1074/jbc.272.37.23042

826 Lendenmann M. H., D. Croll, E. L. Stewart, and B. A. McDonald, 2014 Quantitative trait locus
827 mapping of melanization in the plant pathogenic fungus *Zymoseptoria tritici*. G3
828 GenesGenomesGenetics 4: 2519–2533. https://doi.org/10.1534/g3.114.015289

829 Lendenmann M. H., D. Croll, and B. A. McDonald, 2015 QTL mapping of fungicide sensitivity
830 reveals novel genes and pleiotropy with melanization in the pathogen *Zymoseptoria*
831 *tritici*. Fungal Genet. Biol. 80: 53–67. https://doi.org/10.1016/j.fgb.2015.05.001

832 Li M., X. Liu, Z. Liu, Y. Sun, M. Liu, *et al.*, 2016 Glycoside Hydrolase MoGls2 Controls
833 Asexual/Sexual Development, Cell Wall Integrity and Infectious Growth in the Rice
834 Blast Fungus, (Z. Wang, Ed.). PLOS ONE 11: e0162243.
835 https://doi.org/10.1371/journal.pone.0162243

836 Li D., L. Qin, Y. Wang, Q. Xie, N. Li, *et al.*, 2019 Aflste20 regulates morphogenesis, stress
837 response, and aflatoxin biosynthesis of *Aspergillus flavus*. Toxins 11: 730.
838 https://doi.org/10.3390/toxins11120730

839 Li S., S. Zhang, B. Li, and H. Li, 2021 The snare protein CfVam7 is required for growth,
840 endoplasmic reticulum stress response, and pathogenicity of colletotrichum
841 fructicola. Front. Microbiol. 12: 736066. https://doi.org/10.3389/fmicb.2021.736066

842 Liao Y., G. K. Smyth, and W. Shi, 2019 The R package Rsubread is easier, faster, cheaper and
843 better for alignment and quantification of RNA sequencing reads. Nucleic Acids Res.
844 47: e47–e47. https://doi.org/10.1093/nar/gkz114

845 Macovei A., N. Vaid, S. Tula, and N. Tuteja, 2012 A new DEAD-box helicase ATP-binding
846 protein (OsABP) from rice is responsive to abiotic stress. Plant Signal. Behav. 7:
847 1138–1143. https://doi.org/10.4161/psb.21343

848 Malosetti M., F. A. van Eeuwijk, M. P. Boer, A. M. Casas, M. Elía, *et al.*, 2011 Gene and QTL
849 detection in a three-way barley cross under selection by a mixed model with kinship
850 information using SNPs. Theor. Appl. Genet. 122: 1605–1616.
851 https://doi.org/10.1007/s00122-011-1558-z

852 Mazáň M., K. Mazáňová, and V. Farkaš, 2008 Phenotype analysis of Saccharomyces
853 cerevisiae mutants with deletions in Pir cell wall glycoproteins. Antonie Van
854 Leeuwenhoek 94: 335–342. https://doi.org/10.1007/s10482-008-9228-0

855 Nakamura T., Y. Muramoto, S. Yokota, A. Ueda, and T. Takabe, 2004 Structural and
856 transcriptional characterization of a salt-responsive gene encoding putative ATP-

857 dependent RNA helicase in barley. Plant Sci. 167: 63–70.
858 https://doi.org/10.1016/j.plantsci.2004.03.001

859 Nguyen L., H.-Y. Seok, D.-H. Woo, S.-Y. Lee, and Y.-H. Moon, 2018 Overexpression of the
860 DEAD-Box RNA helicase gene AtRH17 confers tolerance to salt stress in Arabidopsis.
861 Int. J. Mol. Sci. 19: 3777. https://doi.org/10.3390/ijms19123777

862 Oddon D. M., E. Diatloff, and S. K. Roberts, 2007 A CLC chloride channel plays an essential
863 role in copper homeostasis in *Aspergillus nidulans* at increased extracellular copper
864 concentrations. Biochim. Biophys. Acta BBA - Biomembr. 1768: 2466–2477.
865 https://doi.org/10.1016/j.bbamem.2007.05.022

866 Omrane S., H. Sghyer, C. Audéon, C. Lanen, C. Duplaix, *et al.*, 2015 Fungicide efflux and the
867 MgMFS1 transporter contribute to the multidrug resistance phenotype in *Z*
868 *ymoseptoria tritici* field isolates: Fungicide efflux & *MgMFS 1* contribute to MDR in *Z.*
869 *tritici*. Environ. Microbiol. 17: 2805–2823. https://doi.org/10.1111/1462-2920.12781

870 Palma-Guerrero J., X. Ma, S. F. F. Torriani, M. Zala, C. S. Francisco, *et al.*, 2017 Comparative
871 transcriptome analyses in *Zymoseptoria tritici* reveal significant differences in gene
872 expression among strains during plant infection. Mol. Plant-Microbe Interactions®
873 30: 231–244. https://doi.org/10.1094/MPMI-07-16-0146-R

874 Pandey S., A. Prasad, N. Sharma, and M. Prasad, 2020 Linking the plant stress responses
875 with RNA helicases. Plant Sci. 299: 110607.
876 https://doi.org/10.1016/j.plantsci.2020.110607

877 Plissonneau C., A. Stürchler, and D. Croll, 2016 The evolution of orphan regions in genomes
878 of a fungal pathogen of wheat, (J. W. Taylor, Ed.). mBio 7.
879 https://doi.org/10.1128/mBio.01231-16

880 Plissonneau C., F. E. Hartmann, and D. Croll, 2018 Pangenome analyses of the wheat
881 pathogen *Zymoseptoria tritici* reveal the structural basis of a highly plastic eukaryotic
882 genome. BMC Biol. 16: 5. https://doi.org/10.1186/s12915-017-0457-4

883 R Core Team, 2020 R: A language and environment for statistical computing.

884 Richards A., V. Veses, and N. A. R. Gow, 2010 Vacuole dynamics in fungi. Fungal Biol. Rev.
885 24: 93–105. https://doi.org/10.1016/j.fbr.2010.04.002

886 Robinson M. D., D. J. McCarthy, and G. K. Smyth, 2010 edgeR: a Bioconductor package for
887 differential expression analysis of digital gene expression data. Bioinformatics 26:
888 139–140. https://doi.org/10.1093/bioinformatics/btp616

889 RStudio Team, 2020 Rstudio: integrated development environment for R

890 Shi D., W. Ren, J. Wang, J. Zhang, J. I. Mbadianya, *et al.*, 2021 The transcription factor FgNsf1
891 regulates fungal development, virulence and stress responses in Fusarium
892 graminearum. J. Integr. Agric. 20: 2156–2169. https://doi.org/10.1016/S2095-
893 3119(20)63339-1

894 Son H., A. R. Park, J. Y. Lim, and Y.-W. Lee, 2015 Fss1 is involved in the regulation of an *ENA5*
895 homologue for sodium and lithium tolerance in *F usarium graminearum*: Roles of
896 Fss1 in *Fusarium graminearum*. Environ. Microbiol. 17: 2048–2063.
897 https://doi.org/10.1111/1462-2920.12757

898 Wangsanut T., and M. Pongpom, 2022 The role of the glutathione system in stress
899 adaptation, morphogenesis and virulence of pathogenic fungi. Int. J. Mol. Sci. 23:
900 10645. https://doi.org/10.3390/ijms231810645

901 Wu T., E. Hu, S. Xu, M. Chen, P. Guo, *et al.*, 2021 clusterProfiler 4.0: A universal enrichment
902 tool for interpreting omics data. The Innovation 2: 100141.
903 https://doi.org/10.1016/j.xinn.2021.100141

904 Zhan J., C. C. Linde, T. Jurgens, U. Merz, F. Steinebrunner, *et al.*, 2005 Variation for neutral
905 markers is correlated with variation for quantitative traits in the plant pathogenic
906 fungus Mycosphaerella graminicola. Mol. Ecol. 14: 2683–2693.
907 https://doi.org/10.1111/j.1365-294X.2005.02638.x

908 Zhang X., X. Zhao, C. Feng, N. Liu, H. Feng, *et al.*, 2014 The cloning and characterization of a
909 DEAD-Box RNA helicase from stress-responsive wheat. Physiol. Mol. Plant Pathol. 88:
910 36–42. https://doi.org/10.1016/j.pmpp.2014.07.004

911 Zheng P., L. Chen, S. Zhong, X. Wei, Q. Zhao, *et al.*, 2020 A Cu-only superoxide dismutase
912 from stripe rust fungi functions as a virulence factor deployed for counter defense
913 against host-derived oxidative stress. Environ. Microbiol. 22: 5309–5326.
914 https://doi.org/10.1111/1462-2920.15236

915 Zhong Z., T. C. Marcel, F. E. Hartmann, X. Ma, C. Plissonneau, *et al.*, 2017 A small secreted
916 protein in *Zymoseptoria tritici* is responsible for avirulence on wheat cultivars
917 carrying the *Stb6* resistance gene. New Phytol. 214: 619–631.
918 https://doi.org/10.1111/nph.14434

919 Zhong Z., B. A. McDonald, and J. Palma-Guerrero, 2021 Tolerance to oxidative stress is
920 associated with both oxidative stress response and inherent growth in a fungal
921 wheat pathogen, (D. Nielsen, Ed.). Genetics 217: iyaa022.
922 https://doi.org/10.1093/genetics/iyaa022

923 Zhu X., and P. R. Williamson, 2003 A CLC-type chloride channel gene is required for laccase
924 activity and virulence in *Cryptococcus neoformans*: CLC-A of *Cryptococcus*
925 *neoformans*. Mol. Microbiol. 50: 1271–1281. https://doi.org/10.1046/j.1365-
926 2958.2003.03752.x

927
928

929 **Figure 1.** Trait variation in the control and salt stress environments across offspring in each
930 cross. Top panel: Points are mean colony radius in the control and KCl environments at 8
931 and 12 dpi, smoothed lines demonstrate linear change over time. Middle panel: Points are
932 mean grey value in the control and KCL environments at 8 and 12 dpi, smoothed lines
933 demonstrate linear change over time. Bottom panel: Growth rate KCl tolerance and
934 melanisation rate KCl tolerance (KCl tolerance = rate in KCl/rate in control conditions)
935 between the two crosses.
936
937 **Figure 2.** LOD plots from interval mapping for representative traits a) growth rate and b)
938 melanisation rate in the control environment (grey) and in the KCl environment (orange) in
939 the 3D7x3D1 cross. Each sub-panel is a chromosome with the chromosome number
940 indicated at the top. Some numbers are missing because *Zymoseptoria tritici* carries eight
941 accessory chromosomes (Chr 14-21) that show presence/absence polymorphisms among
942 isolates. The dashed horizontal lines indicate the LOD significance thresholds for each trait
943 based on permutation. The numbers above the QTL peaks correspond to the QTL numbers
944 from Table 2. For LOD plots of all traits see Supplementary Information Figure S3.
945
946 **Figure 3**. LOD plots from interval mapping for representative traits a) growth rate and b)
947 melanisation rate in the control environment (grey) and in the KCl environment (orange) in
948 the 1A5x1E4 cross. Some numbers are missing because *Zymoseptoria tritici* carries eight
949 accessory chromosomes (Chr 14-21) that show presence/absence polymorphisms among
950 isolates. The dashed horizontal lines indicate the LOD significance thresholds for each trait
951 based on permutation. The numbers above the QTL peaks correspond to the QTL numbers
952 from Table 3. For LOD plots of all traits see Supplementary Figure S4.
953
954 **Figure 4.** QTL on Chromosome 3 for three traits related to growth under osmotic stress in
955 the 3D7x3D1 cross. The three traits were colony radius at 8 dpi, colony radius KCl tolerance
956 at 8 and 12 dpi (KCl tolerance = colony radius in KCl/colony radius in control conditions). A)
957 LOD peak and Bayes credible interval (shaded) from interval mapping, with SNP positions
958 indicated on the x-axis as black vertical lines, b) Alignment of the 36 genes within the QTL
959 interval between the 3D7 and 3D1 parental strains – orange-coloured genes are the six most
960 promising candidate genes described in the main text and c) allelic effects of 94 SNPs within

961 the QTL interval on mean colony radius in KCl at 8 dpi. Isolates carrying the reference allele
962 (ref=3D7) shown in grey have smaller colonies compared to the alternative allele (alt=3D1)
963 shown in orange. SNP position in base pairs is shown on the x-axis. The marker with the
964 highest LOD is at position 737773 bp.
965
966 **Supplementary Figures**
967 Figure S1. Correlation of growth rate and melanisation rate in control and KCl environment.
968 Figure S2. Correlation of mean radius and mean grey value ar 12 dpi in control and KCl
969 environment.
970 Figure S3. LOD plots from interval mapping for all traits in the 3D7x3D1 cross.
971 Figure S4. LOD plots from interval mapping for all traits in the 1A5x1E4 cross.
972
973
974 **Supplementary Tables**
975 Table S1. Linkage map summary
976 Table S2. Summary of phenotypic data
977 Table S3. Trait correlations in 3D7x3D1 cross.
978 Table S4. Trait correlations in 1A5x1E4 cross.
979 Table S5. Results of the GO enrichment analysis for 3D7x3D1 cross.
980 Table S6. Results of the GO enrichment analysis for 1A5x1E4 cross.
981 Table S7. GO enrichment genes.
982 Table S8. QTL interval on Chr 3 (QTL#3) in 3D7x3D1 cross in detail.
983 Table S9. Results of the SNP effect analysis for the QTL interval on Chr 3 (QTL #3)

Table 1. Summary of the QTL mapping results for all traits. Grey value and colony radius were measured at two time points: 8 and 12 dpi. Growth rate was calculated as the change in colony radius/number of days. Melanisation rate was calculated as the change in grey value/number of days. Colony radius/grey value KCl tolerance were calculated by dividing the value (grey value or colony radius) in the control environment by the value in the KCl environment. Growth rate/Melanisation KCl tolerance were calculated by dividing the rate (melanisation or growth) in the control environment by the rate in the KCl environment. The QTL peak columns show the chromosomal position of significant QTL peak for each trait in the 3D7x3D1 and 1A5x1E4 crosses respectively, and the final column contains estimated heritability (h^2) for each trait.

Data Type	Environment	DPI	Trait	Trait Full Name	QTL peak 3D7x3D1	h^2	QTL peak 1A5x1E4	h^2
Time point	Control	8	Colony radius	Colony radius in Control at 8dpi	3,8,10,11	0.53	2,3,8	0.56
Time point	Control	12	Colony radius	Colony radius in Control at 12dpi	3,7,8,10,11	0.62	7,8	0.48
Time point	KCl	8	Colony radius	Colony radius in KCl at 8dpi	3,4	0.64	6,	0.50
Time point	KCl	12	Colony radius	Colony radius in KCl at 12dpi	3,8	0.60	1,8	0.52
Time point	Control	8	Grey value	Grey value in Control at 8dpi	8,10,11	0.42	1,2,3,8	0.63
Time point	Control	12	Grey value	Grey value in Control at 12dpi	11	0.22	2,3,8	0.44
Time point	KCl	8	Grey value	Grey value in KCl at 8dpi	8,11	0.54	8	0.34
Time point	KCl	12	Grey value	Grey value in KCl at 12dpi	1,2,11	0.34	No Sig. QTL	0.29
Rate	Control	8-12	Growth rate	Growth rate in Control	3,8,11	0.61	7,8	0.33
Rate	KCl	8-12	Growth rate	Growth rate in KCl	3,8,11	0.45	8,	0.49
Rate	Control	8-12	Melanisation rate	Melanisation rate in Control	10	0.28	2,3,12	0.54
Rate	KCl	8-12	Melanisation rate	Melanisation rate in KCl	1,6	0.32	No Sig. QTL	0.27
Tolerance	Both	8	Grey value	Grey value KCl tolerance at 8 dpi	8,10	0.37	1,2,3,8	0.58
Tolerance	Both	12	Grey value	Grey value KCl tolerance at 12 dpi	11	0.18	No Sig. QTL	0.34
Tolerance	Both	8	Colony radius	Colony radius KCl tolerance at 8dpi	3,4,10	0.59	8	0.42
Tolerance	Both	12	Colony radius	Colony radius KCl tolerance at 12dpi	3,10,11	0.47	1	0.37
Tolerance	Both	8-12	Growth rate	Growth rate KCl tolerance	11	0.40	1,5	0.45
Tolerance	Both	8-12	Melanisation rate	Melanisation rate KCl tolerance	1	0.14	No Sig. QTL	0.32

Table 2. Description of all QTL identified from the 3D7x3D1 cross, including map and physical position of the LOD peak marker, the Bayes credible interval length and the number of genes within the interval. PVE is the proportion of variance explained by the QTL. QTL number is a number assigned to a particular QTL peak which groups overlapping QTLs. Superscript letters indicate QTL unique to KCL environment for size-related (^{S}) and melanin-related traits (^{M}).

Type	Chr	Pos (cM)	LOD	Pos (bp)	No. markers	Interval Start (bp)	Interval end (bp)	Interval size (bp)	No. Genes	PVE	QTL number
Melanisation rate in KCl	1	457.43	6.18	1590235	2915	1035571	2769729	1734.158	598	0.10	1 ^{M}
Melanisation rate KCl tolerance	1	540.00	3.40	2295356	9000	788430	6389989	5601.559	1977	0.06	1 ^{M}
Grey value in KCl at 12dpi	1	576.00	5.99	2717234	519	2295128	2769729	474.601	174	0.10	1 ^{M}
Grey value in KCl at 12dpi	2	261.00	5.07	691536	141	679366	711981	32.615	15	0.09	2 ^{M}
Colony radius KCl tolerance at 12dpi	3	142.92	4.49	719549	553	396401	944712	548.311	125	0.08	3 ^{S}
Colony radius KCl tolerance at 8dpi	3	144.00	14.62	737773	105	588483	751983	163.5	36	0.23	3 ^{S}
Colony radius in KCl at 8dpi	3	144.15	22.83	737773	94	588483	737773	149.29	31	0.33	3 ^{S}
Growth rate in Control	3	415.00	5.31	2537296	2204	1982744	3347765	1365.021	462	0.09	4
Colony radius in Control at 12dpi	3	456.63	8.11	2993469	427	2971359	3196103	224.744	79	0.13	4
Colony radius in Control at 8dpi	3	482.67	7.09	3056536	428	2982086	3199430	217.344	76	0.12	4
Growth rate in KCl	3	485.65	4.93	3110053	845	2971359	3347765	376.406	132	0.08	4
Colony radius in KCl at 12dpi	3	485.65	4.99	3110053	3084	516017	3203947	2687.93	813	0.08	4
Colony radius KCl tolerance at 8dpi	4	400.00	4.28	1936846	1000	1845763	2448166	602.403	200	0.07	5 ^{S}
Colony radius in KCl at 8dpi	4	403.76	4.37	2013908	986	1867509	2448166	580.657	194	0.07	5 ^{S}
Melanisation rate in KCl	6	220.14	6.24	1767543	479	1568163	1981193	413.03	124	0.10	6 ^{M}
Colony radius in Control at 12dpi	7	186.78	4.47	1109088	1366	511101	1377451	866.35	265	0.08	7
Grey value in KCl at 8dpi	8	680.87	5.69	943669	732	502305	974947	472.642	123	0.10	8 ^{M}
Growth rate in Control	8	746.72	7.31	1100862	542	1071962	1221280	149.318	65	0.12	9
Colony radius in Control at 12dpi	8	746.72	10.77	1100862	274	1091579	1164224	72.645	29	0.17	9
Growth rate in KCl	8	747.72	9.66	1100862	667	1091692	1284370	192.678	77	0.16	9
Colony radius in KCl at 12dpi	8	751.61	9.79	1112633	670	1100862	1292397	191.535	76	0.16	9
Colony radius in Control at 8dpi	8	765.72	8.04	1221337	751	1091475	1354349	262.874	108	0.13	9

Grey value KCl tolerance at 8dpi	8	776.11	4.22	1350673	2608	962119	2165894	1203.775	457	0.07	9
Grey value in Control at 8dpi	8	776.11	4.35	1350706	2549	981398	2175005	1193.607	450	0.07	9
Grey value in Control at 8dpi	10	199.98	12.37	775475	160	769669	861699	92.03	32	0.20	10
Grey value KCl tolerance at 8dpi	10	199.98	10.68	775475	281	769669	919978	150.309	56	0.17	10
Melanisation rate in KCl	10	200.35	8.66	792011	299	769669	924425	154.756	59	0.14	10
Colony radius in Control at 8dpi	10	200.72	12.32	792272	299	769669	924425	154.756	59	0.19	10
Colony radius KCl tolerance at 8dpi	10	211.51	10.58	924412	283	792019	924425	132.406	53	0.17	10
Colony radius KCl tolerance at 12dpi	10	211.51	6.68	924414	1081	749521	1302645	553.124	211	0.11	10
Colony radius in Control at 12dpi	10	212.61	4.92	924425	540	749521	1054575	305.054	116	0.08	10
Colony radius in Control at 8dpi	11	183.07	4.20	507361	528	311631	698718	387.087	128	0.07	11
Colony radius KCl tolerance at 12dpi	11	188.28	5.60	581439	1340	74200	890544	816.344	268	0.09	11
Grey value in KCl at 12dpi	11	192.28	6.87	605810	408	463714	776764	313.05	99	0.11	11
Growth rate in Control	11	193.00	19.63	616039	5	616039	658119	42.08	13	0.29	11
Growth rate in KCl	11	193.00	5.47	616039	219	468760	698718	229.958	72	0.09	11
Colony radius in Control at 12dpi	11	193.00	16.79	616039	25	601600	658119	56.519	16	0.26	11
Grey value in Control at 12dpi	11	194.11	6.64	657530	498	514049	870059	356.01	121	0.11	11
Grey value KCl tolerance at 12dpi	11	194.11	5.55	657530	700	367519	870059	502.54	168	0.09	11
Grey value in Control at 8dpi	11	194.11	5.30	658070	244	463714	704331	240.617	77	0.09	11
Grey value in KCl at 8dpi	11	194.11	17.09	658119	5	616039	658119	42.08	13	0.26	11
Growth rate KCl tolerance	11	195.28	7.45	658119	370	500942	802650	301.708	98	0.12	11

Table 3. Description of all QTLs identified from the 1A5x1E4 cross, including map and physical position of the LOD peak marker, the Bayes credible interval length and the number of genes within the interval. PVE is the proportion of variance explained by the QTL. QTL number is a number assigned to a particular QTL peak which identifies overlapping QTLs. Superscript letters indicate QTL unique to KCL environment for size-related (^{S}) and melanin-related traits (^{M}).

Type	Chr	Pos (cM)	LOD	Pos (bp)	No. markers	Interval Start (bp)	Interval end (bp)	Interval size (bp)	No. Genes	PVE	QTL number
Grey value in Control at 8dpi	1	328.91	5.69	572065	402	442697	727696	284.999	92	0.10	1
Grey value KCl tolerance at 8dpi	1	328.91	5.01	572065	405	442697	732023	289.326	93	0.08	1
Melanisation rate KCl tolerance	1	328.91	4.46	572065	463	461577	779936	318.359	102	0.08	1
Colony radius KCl tolerance at 12dpi	1	559.12	4.07	1849200	4654	399579	5725682	5326.103	1964	0.07	2 ^{S}
Growth rate KCl tolerance	1	797.00	4.80	3405315	3068	399544	3488556	3089.012	1151	0.08	2 ^{S}
Colony radius in KCl at 12dpi	1	1104.00	4.03	5792644	4774	372886	5956797	5583.911	2056	0.07	2 ^{S}
Melanisation rate in Control	2	70.00	6.56	574965	1211	405115	1914465	1509.35	509	0.11	3
Grey value in Control at 12dpi	2	204.66	4.55	1438934	618	1284536	2152463	867.927	281	0.08	4
Grey value in Control at 8dpi	2	204.66	18.08	1438934	185	1438863	1748215	309.352	95	0.27	4
Grey value KCl tolerance at 8dpi	2	204.66	15.97	1438934	184	1438934	1748215	309.281	95	0.24	4
Colony radius in Control at 8dpi	2	211.42	8.76	1631840	217	1438934	1776132	337.198	105	0.14	4
Grey value KCl tolerance at 8dpi	3	147.00	6.15	1325440	210	1243932	1684531	440.599	179	0.10	5
Grey value in Control at 8dpi	3	148.00	6.66	1325440	133	1325422	1592801	267.379	115	0.11	5
Colony radius in Control at 8dpi	3	163.74	5.83	1521535	725	355042	1592801	1237.759	374	0.10	5
Melanisation rate in Control	3	193.38	11.99	1711037	290	1489966	2105601	615.635	180	0.19	6
Grey value in Control at 12dpi	3	198.73	4.04	1928783	860	1743111	2927356	1184.245	361	0.07	6
Growth rate KCl tolerance	5	399.00	4.34	2638913	155	2511016	2658480	147.464	48	0.07	7 ^{S}
Colony radius in KCl at 8dpi	6	179.00	4.48	1512508	594	778583	1557528	778.945	256	0.08	8 ^{S}
Growth rate in Control	7	158.82	4.43	539824	255	437699	651318	213.619	80	0.07	9
Colony radius in Control at 12dpi	7	158.82	4.67	539837	254	437718	651318	213.6	80	0.08	9
Growth rate in KCl	8	76.80	8.79	274792	82	256529	346224	89.695	25	0.14	10
Colony radius in KCl at 12dpi	8	76.80	8.94	274792	67	256529	313758	57.229	17	0.15	10

Grey value in Control at 12dpi	8	78.58	4.92	302772	882	89684	921404	831.72	308	0.08	10
Grey value in Control at 8dpi	8	79.00	12.12	302772	66	270834	346224	75.39	22	0.19	10
Colony radius in Control at 12dpi	8	79.00	9.72	302772	80	260355	346224	85.869	24	0.16	10
Colony radius in Control at 8dpi	8	79.00	11.06	302772	415	260101	732444	472.343	163	0.18	10
Grey value KCl tolerance at 8dpi	8	79.00	8.26	302772	339	89573	346224	256.651	90	0.14	10
Colony radius KCl tolerance at 8dpi	8	137.00	5.05	832180	1177	589084	1648406	1059.322	396	0.08	10
Grey value in KCl at 8dpi	8	164.00	4.33	1377926	1406	305075	1623437	1318.362	485	0.07	10
Melanisation rate in Control	12	126.74	4.24	473688	275	441706	821603	379.897	101	0.07	11

Table 4 Genes within the QTL interval for colony radius at 8 dpi in KCl and colony radius KCl tolerance at 8 dpi in the 3D7x3D1 cross. Bold indicates genes that are the most promising candidate genes, as described in the main text. Gene sequence similarity between the two parental strains was obtained using BLAST. DGE: Differential gene expression column indicates if the gene was differentially expressed between parents in any one of the data sets used (in planta or in vitro, see Methods in main text). The annotations were obtained using Interproscan using multiple protein databases, here we show only the PFAM annotation.

Chr	Gene id 3D7	Gene start	Gene end	Gene id 3D1	Sequence similarity (%)	DGE	**Annotation**
3	**ZT3D7_G3622**	**598091**	**599743**	**ZT3D1_G3567**	**97.68**	**yes**	**Fungal-specific transcription factor domain**
3	ZT3D7_G3623	637954	638542	ZT3D1_G7387	96.23	NA	
3	ZT3D7_G3624	653468	654397	ZT3D1_G3569	90.78	yes	Protein of unknown function (DUF1349)
3	ZT3D7_G3625	655237	656628	ZT3D1_G3570	97.04	yes	
3	ZT3D7_G3626	667030	667567	NA		yes	Pterin 4 alpha carbinolamine dehydratase
3	ZT3D7_G3627	667812	668321	ZT3D1_G3571	98.46	yes	
3	ZT3D7_G3628	670445	671787	ZT3D1_G3572	100.00	yes	Transketolase, pyrimidine binding domain, Transketolase, C-terminal domain
3	ZT3D7_G3629	672336	673658	ZT3D1_G3573	99.83	NA	
3	ZT3D7_G3630	674777	676658	ZT3D1_G3574	99.96	yes	Dehydratase family
3	ZT3D7_G3631	677782	680135	ZT3D1_G3576	97.72	yes	ABC transporter, ABC transporter
3	ZT3D7_G3632	680734	681942	ZT3D1_G3577	97.73	yes	Epoxide hydrolase N terminus
3	ZT3D7_G3633	683647	685131	ZT3D1_G3578	81.12	NA	Phosphotransferase enzyme family
3	ZT3D7_G3634	685575	685937	ZT3D1_G3579	98.96	yes	
3	**ZT3D7_G3635**	**686721**	**692363**	**ZT3D1_G3580**	**99.07**	**yes**	**Protein kinase domain, Protein kinase C terminal domain, N-terminal half of MaoC dehydratase, MaoC like domain, C2 domain**
3	ZT3D7_G3636	693114	696535	ZT3D1_G3582	99.50	yes	Importin-beta N-terminal domain, Cse1
3	**ZT3D7_G3637**	**697014**	**700871**	**ZT3D1_G3583**	**97.44**	**yes**	**DEAD/DEAH box helicase, rRNA-processing arch domain, DSHCT (NUC185) domain, Ski2 N-terminal region, Helicase conserved C-terminal domain**
3	ZT3D7_G3638	701182	702047	ZT3D1_G3584	98.74	yes	short chain dehydrogenase
3	**ZT3D7_G3639**	**702431**	**704143**	**ZT3D1_G3585**	**97.16**	**yes**	**Major Facilitator Superfamily**
3	ZT3D7_G3640	705425	706303	ZT3D1_G3587	99.91	yes	
3	ZT3D7_G3641	706740	707975	ZT3D1_G3588	98.53	yes	
3	ZT3D7_G3642	708779	709336	ZT3D1_G3589	98.33	NS	
3	ZT3D7_G3643	709874	711886	ZT3D1_G3590	94.46	yes	Ubiquitin-conjugating enzyme
3	ZT3D7_G3644	712327	715212	ZT3D1_G3591	98.93	yes	Utp14 protein
3	ZT3D7_G3645	715430	715798	ZT3D1_G3592	99.74	no	Mitochondrial ribosomal protein L27

3	ZT3D7_G3646	716302	720497	ZT3D1_G3593	98.96	NA	Staphylococcal nuclease homologue, short chain dehydrogenase, Enoyl-(Acyl carrier protein) reductase, Tudor domain
3	ZT3D7_G3647	720900	723737	ZT3D1_G3594	99.38	yes	PQQ-like domain, ER membrane protein complex subunit 1, C-terminal
3	ZT3D7_G3648	725571	726437	ZT3D1_G3595	99.02	no	Ras family
3	ZT3D7_G3649	726651	727599	NA		yes	NmrA-like family
3	ZT3D7_G3650	727935	729979	ZT3D1_G3596	98.53	no	Heterokaryon incompatibility protein (HET)
3	ZT3D7_G3651	730698	731819	ZT3D1_G3597	99.93	yes	Transaldolase/Fructose-6-phosphate aldolase
3	ZT3D7_G3652	732329	733083	ZT3D1_G3598	96.53	yes	Copper/zinc superoxide dismutase (SODC)
3	ZT3D7_G3653	734230	736078	ZT3D1_G3599	99.73	yes	FGGY family of carbohydrate kinases, C-terminal domain, FGGY family of carbohydrate kinases, N-terminal domain
3	ZT3D7_G3654	737260	737987	ZT3D1_G3600	99.87	yes	
3	**ZT3D7_G3655**	**739211**	**741757**	**ZT3D1_G3601**	**99.97**	**yes**	**CBS domain, Voltage gated chloride channel**
3	ZT3D7_G3656	743352	744442	ZT3D1_G3602	99.73	yes	Protein of unknown function (DUF1295)
3	ZT3D7_G3657	744744	746896	ZT3D1_G3603	99.92	yes	Pro-kumamolisin, activation domain
3	**ZT3D7_G3658**	**748505**	**750639**	**ZT3D1_G3604**	**100**	**yes**	**PX domain, Vps5 C terminal like**

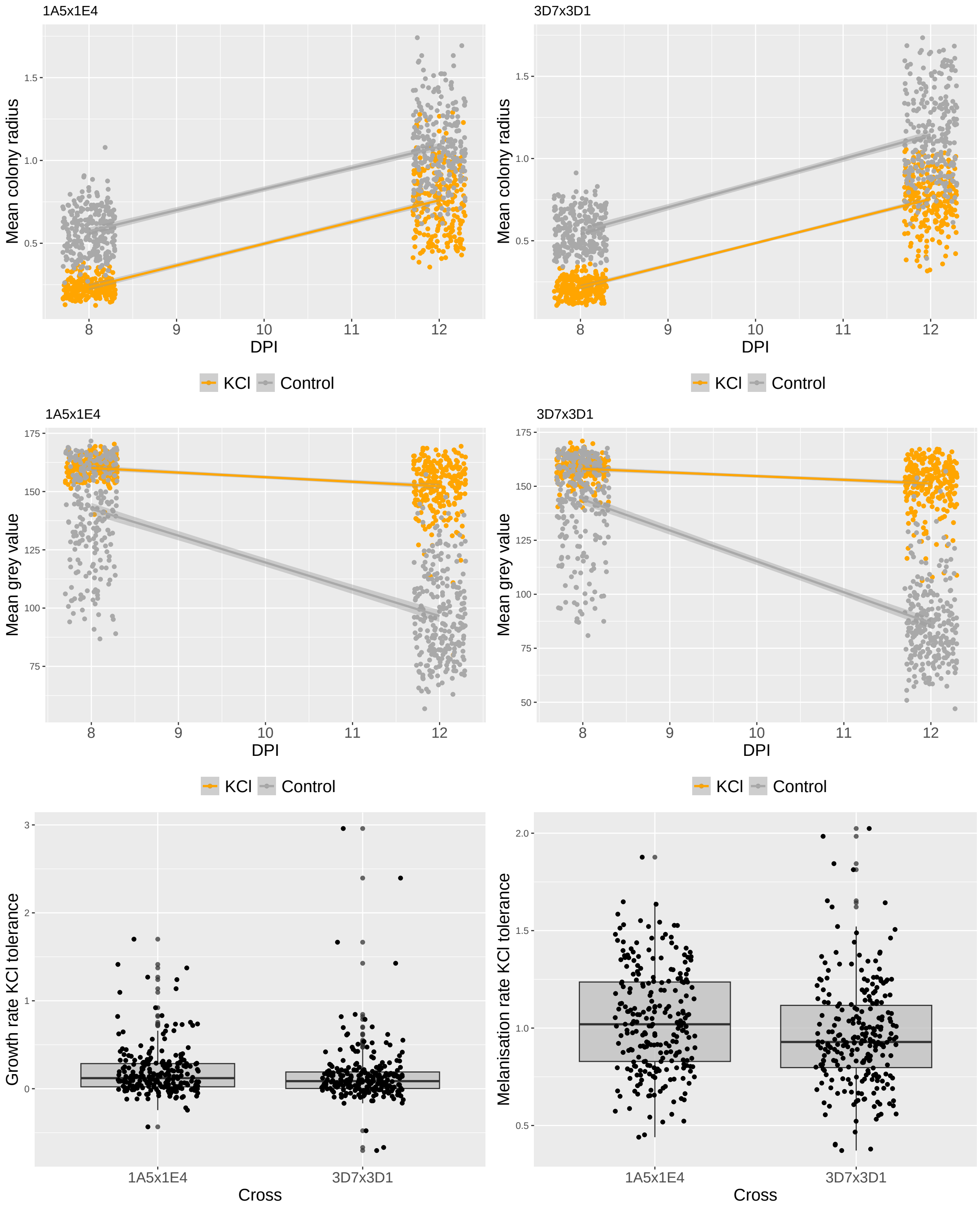
1A5x1E4
3D7x3D1
Mean colony radius
1.5
1.0
0.5
8
9
10
11
12
DPI
KCl
Control
Mean grey value
175
150
125
100
75
50
Growth rate KCl tolerance
3
2
1
0
Melanisation rate KCl tolerance
2.0
1.5
1.0
0.5
Cross

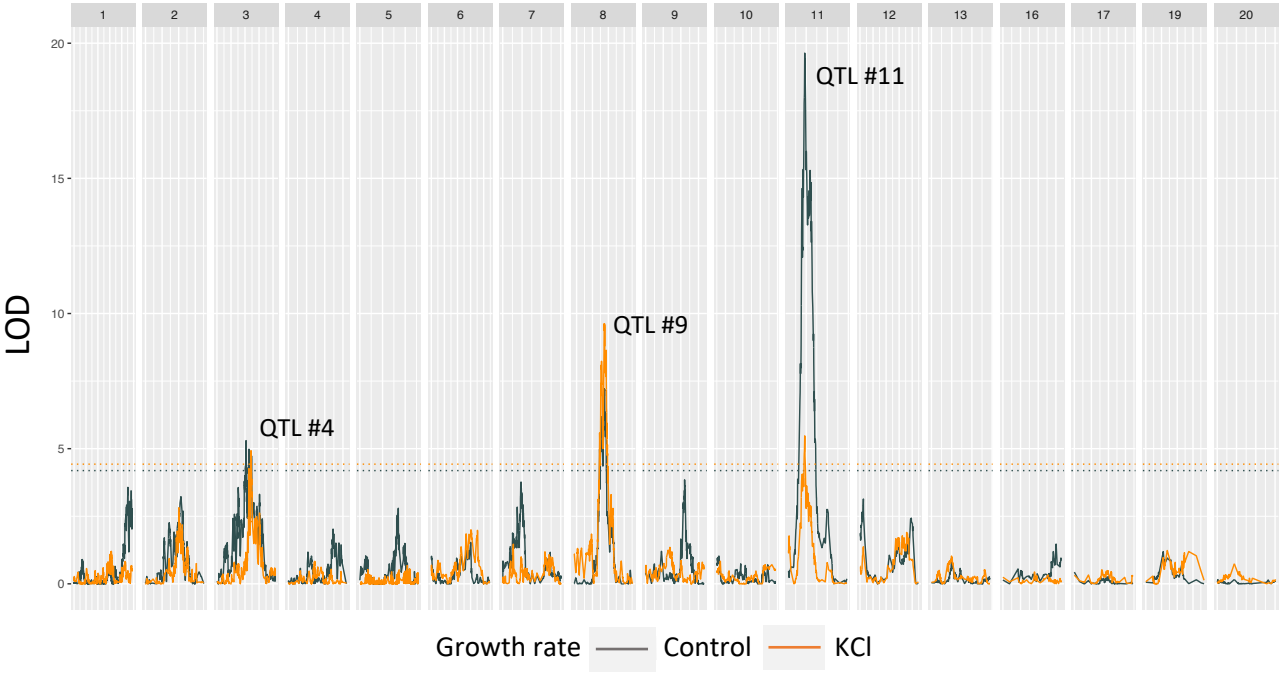
1
2
3
4
5
6
7
8
9
10
11
12
13
16
17
19
20
LOD
20
15
10
5
0
QTL #11
QTL #9
QTL #4
Growth rate
Control
KCl

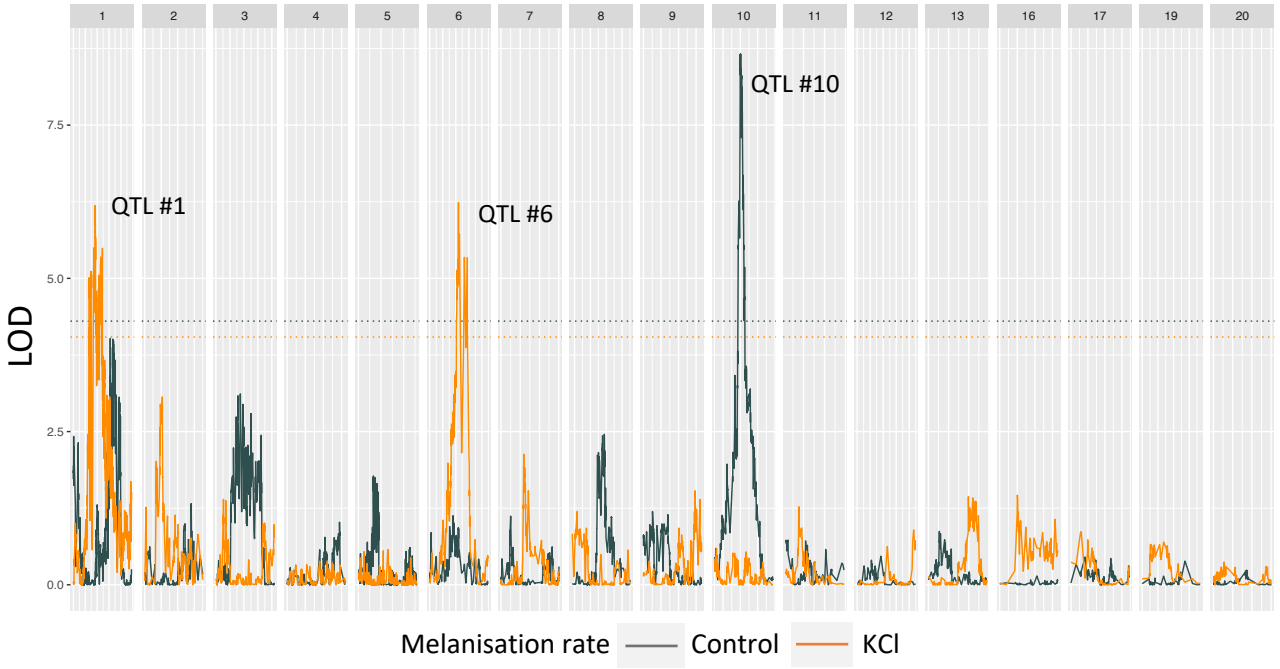
1
2
3
4
5
6
7
8
9
10
11
12
13
16
17
19
20
LOD
7.5
5.0
2.5
0.0
QTL #10
QTL #1
QTL #6
Melanisation rate
Control
KCl

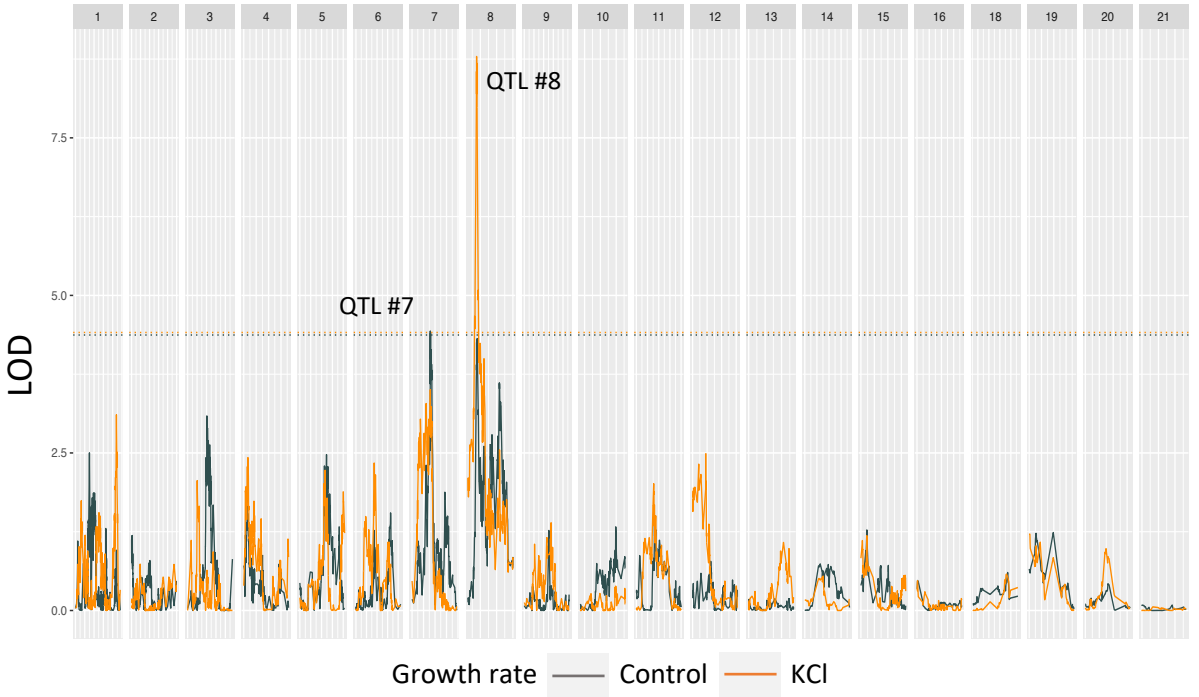
1
2
3
4
5
6
7
8
9
10
11
12
13
14
15
16
18
19
20
21
QTL #8
QTL #7
LOD
7.5
5.0
2.5
0.0
Growth rate
Control
KCl

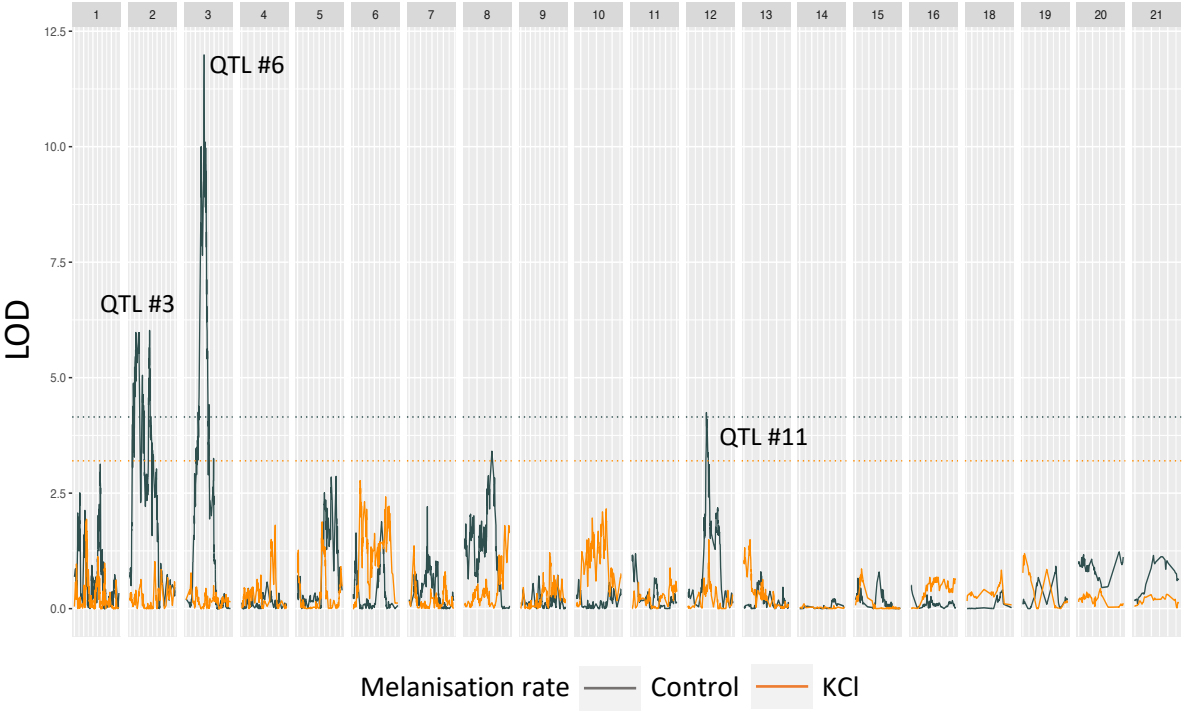
1
2
3
4
5
6
7
8
9
10
11
12
13
14
15
16
18
19
20
21
QTL #6
QTL #3
QTL #11
LOD
12.5
10.0
7.5
5.0
2.5
0.0
Melanisation rate
Control
KCl

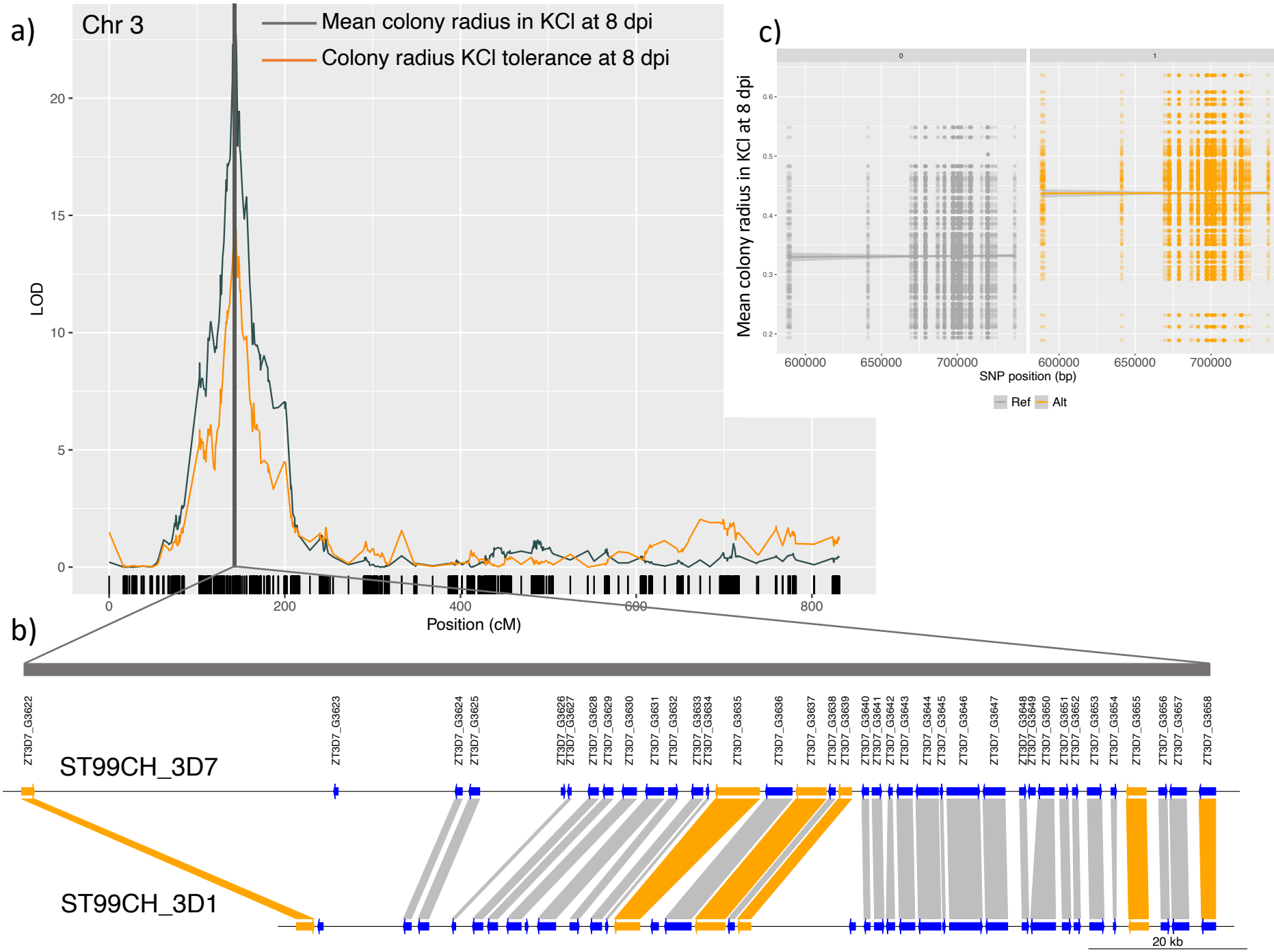
a)
Chr 3
Mean colony radius in KCl at 8 dpi
Colony radius KCl tolerance at 8 dpi
LOD
Position (cM)
c)
Mean colony radius in KCl at 8 dpi
SNP position (bp)
Ref
Alt
b)
ST99CH_3D7
ST99CH_3D1
20 kb